Distribution of Vesicular Glutamate Transporter 2 (VGluT2) in the Primary Visual Cortex of the Macaque and Human

Virginia Garcia-Marin,* Tunazzina H. Ahmed, Yasmeen C. Afzal, and Michael J. Hawken

Center for Neural Science, New York University, New York, New York 10003

ABSTRACT

The majority of thalamic terminals in V1 arise from lateral geniculate nucleus (LGN) afferents. Thalamic afferent terminals are preferentially labeled by an isoform of the vesicular glutamate transporter, VGluT2. The goal of our study was to determine the distribution of VGluT2-ir puncta in macaque and human visual cortex. First, we investigated the distribution of VGluT2-ir puncta in all layers of macaque monkey primary visual cortex (V1), and found a very close correspondence between the known distribution of LGN afferents from previous studies and the distribution of VGluT2-immunoreactive (-ir) puncta. There was also a close correspondence between cytochrome oxidase density and VGluT2-ir puncta distribution. After validating the correspondence in macaque, we made a comparative study in human V1. In many aspects, the distribution of VGluT2-ir puncta in human was qualitatively similar to that of the macaque: high densities in layer 4C, patches of VGluT2-ir puncta in the supragranular layer (2/3), lower but clear distribution in layers 1 and 6, and very few puncta in layers 5 and 4B. However, there were also important differences between macaques and humans. In layer 4A of human, there was a sparse distribution of VGluT2-ir puncta, whereas in macaque, there was a dense distribution with the characteristic honeycomb organization. The results suggest important changes in the pattern of cortical VGluT2 immunostaining that may be related to evolutionary differences in the cortical organization of LGN afferents between Old World monkeys and humans. J. Comp. Neurol. 521:130–151, 2013.

INDEXING TERMS: thalamic afferents; V1 cortical layers; cytochrome oxidase

Understanding the relative distribution of thalamic afferent and intracortical terminals is an important component in defining the cortical microcircuit (Lund, 1988; Douglas and Martin, 1991; Callaway, 1998; DeFelipe, 2002). The distribution of afferent terminals is a crucial factor in numerous models of cortical circuits (McLaughlin et al., 2000). The number of afferent terminals changes markedly during development (Mates and Lund, 1983), in amblyopia and in visual deprivation (Hubel et al., 1977). Investigation of non-human primate pathways uses a variety of invasive tract-tracing anatomical methods that are not applicable in human studies, and therefore it has not been feasible to assay the afferent input to visual cortex in humans. With the advent of specific markers for thalamo-cortical terminals that are independent of intracortical terminals, it has become possible to apply these techniques to the human brain, and determine the distribution of afferent terminals, as we have done in this study using an antibody against the vesicular glutamate transporter 2 (VGluT2).

In primary visual cortex (V1), the architecture of Old World monkeys and great apes, including humans, is qualitatively similar, although there are numerous quantitative differences among these species (Horton and Hedley-Whyte, 1984; Preuss et al., 1999; Preuss and Coleman, 2002; DeFelipe et al., 2006). One common

Grant sponsor: National Institutes of Health; Grant numbers: EY17945 and P30EY013079; Grant sponsor: The Spanish Ministry of Education, Science and Innovation; Grant numbers: EX2009-0636 (National R&D&I Plan 2008-2011, National Human Resources Mobility Program, Postdoctoral Mobility in Foreign Centers; to V.G.-M.) and SAF2009-09394.

*CORRESPONDENCE TO: Virginia Garcia-Marin, Center for Neural Science, New York University, 4 Washington Place, New York, NY 10003. E-mail: vgmarin@cns.nyu.edu

Received August 4, 2011; Revised November 18, 2011; Accepted June 4, 2012

DOI 10.1002/cne.23165

Published online June 11, 2012 in Wiley Online Library (wileyonlinelibrary.com)

characteristic of the visual system across these species is the distribution of the three cone photoreceptors (L-, M-, and S-cones) that feed into the different classes of ganglion cells giving rise to the correspondingly elaborate retino-geniculo-cortical pathway (Leventhal et al., 1981; Livingstone and Hubel, 1988; Kaas and Huerta, 1988; Conley and Fitzpatrick, 1989; Casagrande and Norton, 1991; Casagrande, 1994; Hendry and Yoshioka, 1994).

A comprehensive view of the distribution of afferent terminals in the monkey cortex has been assembled over the past 40 years, by using degeneration techniques (Jones and Powell, 1970; Peters and Feldman, 1976; Davis and Sterling, 1979), transneuronal anterograde tracing with ^{3}H-proline from the eye (Wiesel et al., 1974; Hubel et al., 1977), anterograde tracing with ^{3}H-proline and ^{35}S methionine (Hendrickson et al., 1978) and anterograde transport of horseradish peroxidase (HRP), biotinylated dextran amine (BDA) from the lateral geniculate nucleus (LGN) (McGuire et al., 1984; LeVay, 1986; Kharazia and Weinberg, 1993; Ahmed et al., 1994; Herrmann et al., 1994), intracellular injections of tracer into individual axons (Blasdel and Lund, 1983; Friedlander and Martin, 1989; Freund et al., 1989; Anderson et al., 1992), retrograde tracer injections from V1 to the LGN (Hendry and Yoshioka, 1994), and immunocytochemical characterization of parvalbumin (PV) terminals using electron microscopy (EM) (DeFelipe and Jones, 1991; Latawiec et al., 2000).

The combined results of all these studies show that there is a dense terminal distribution in the lower half of layer 4C (4Cβ) arising from the P-pathway that also provides collateral inputs to layer 4A and to the upper half of layer 6. There is a correspondingly dense distribution in the upper half of layer 4C (4Cα) arising from the M-pathway that also provides collateral branches to the lower half of layer 6. Finally, the main input to layer 1, and to the cytochrome oxidase (CO)-rich patches of layers 2 and 3, is provided by the K-pathway, which also contributes to the LGN input to layer 4A (Livingstone and Hubel, 1982; Fitzpatrick et al., 1983; Weber et al., 1983; Lachica and Casagrande, 1992; Hendry and Yoshioka, 1994; Ding and Casagrande, 1997; Casagrande et al., 2007).

The advent of molecular markers that have specificity for different neuronal populations and terminals (e.g., Celio et al., 1986, 1990) has proved extremely useful in characterizing many aspects of visual cortical circuits in different species, including human and non-human primates (DeFelipe, 1997; Preuss and Coleman, 2002; Sherwood et al., 2007). VGluT is particularly useful in this regard; It comes in three main isoforms: VGluT1, VGluT2, and VGluT3. The VGluT1 and VGluT2 isoforms are expressed in subpopulations of well-characterized glutamatergic neurons (Takamori et al., 2000, 2001; Fremeau et al., 2001; Herzog et al., 2001; Varoqui et al., 2002), whereas VGluT3 is expressed in neurons not classically considered glutamatergic (e.g. γ-aminobutyric acid [GABA]ergic, cholinergic, and monoaminergic neurons), suggesting a different role of glutamate transport in these neuronal groups (Fremeau et al., 2001, 2002; Gras et al., 2002; Schafer et al., 2002; Takamori et al., 2002).

A complementary expression of VGluT1 and VGluT2 has been reported in subpopulations of axon terminals or neuronal cell bodies of glutamatergic neurons in the central nervous system (CNS). VGluT1 is expressed mainly in the axon terminals of neurons in the telencephalon, and is principally associated with cortico-cortical projections within the cortex, whereas VGluT2 is primarily utilized by projections from the midbrain, thalamus, brainstem, and spinal cord (Fremeau et al., 2001; Fujiyama et al., 2001, 2003; Boulland et al., 2004; Nahmani and Erisir, 2005; Nakamura et al., 2005; Graziano et al., 2008; Coleman et al., 2010; Kameda et al., 2012; review in Fremeau et al., 2004). Although most studies report no colocalization of VGluT2 and VGluT1, there are a few reports of colocalization (Fyk-Kolodziej et al., 2004; Nakamura et al., 2005; Herzog et al., 2006; Graziano et al., 2008; Balaram and Kaas, 2011). In ferret visual cortex, VGluT2 is localized in thalamo-cortical axon terminals but not in intracortical axon terminals (Nahmani and Erisir, 2005).

We have studied the differential distribution of VGluT2 in V1 of macaque (the commonly used representative of Old World monkeys) and humans. Our results conform closely with the laminar distribution of LGN thalamic afferents terminals in macaque V1. In addition, they show a fluctuating density pattern in layer 6 uncovered by VGluT2 processing that is not evident in CO staining. There have been studies of the afferent terminations in apes (Tigges and Tigges, 1979) and humans (Miklossy, 1992) that indicate substantial input to layer 4C, and a few fibers in layer 6. However, these studies did not show input to other layers, including 4A, 2/3, and 1, possibly because of the sensitivity of the methods. Our results show high density of VGluT2-immunoreactive (-ir) puncta in layer 4C with lower densities in layers 6 and 1, and a repetitive discrete patchy pattern in parts of layers 2 and 3. In addition, our results also show VGluT2-ir puncta in human layer 4A, although there was a substantial reduction in the density in this layer compared with the macaque.

MATERIALS AND METHODS

Macaque brain tissue

Ten, young adult, male, long-tailed macaque monkeys (*Macaca fascicularis*) that had been previously used for anesthetized electrophysiological recordings were used

TABLE 1.
Primary Antibodies Used

Antibody	Source	Manufacturer	Dilution
Vesicular glutamate 1 transporter	Synthetic linear peptide from rat VGluT1	Millipore (Billerica, MA), polyclonal guinea-pig, #AB5905MI	1:2,500
Vesicular glutamate 2 transporter	Recombinant protein from rat VGluT2	Millipore, mouse monoclonal, #MAB5504	1:4,000
NeuN	Purified cell nuclei from mouse brain	Millipore, mouse monoclonal, #MAB377	1:2,000

in this study. Animals were prepared for recording as described elsewhere (Xing et al., 2004; Solomon et al., 2004). After 4–5 days of recordings, experiments were terminated by i.v. injection of a lethal dose of pentobarbital (60 mg/kg), and brain death was determined by a flat electroencephalogram. Subsequently, animals were transcardially perfused with heparinized 0.01 M phosphate-buffered saline (PBS; pH 7.4) followed by 4 L of chilled 4% paraformaldehyde (PFA) in 0.1 M phosphate buffer (PB; pH 7.4). Fixative was run for at least 40 minutes. Some blocks of V1 were removed for track reconstruction of the recording locations of electrophysiologically characterized neurons, and the remaining V1 tissue was cut into small blocks and postfixed in the same fixative for 24–48 hours at 4°C in 4% PFA. After fixation, serial sections (50 and 30 μm, for parasagittal and horizontal sections, respectively) were obtained by using a vibratome, and the sections were batch-processed for immunocytochemical staining. The remaining sections and blocks were immersed in graded sucrose solutions, and were stored in a cryoprotectant solution at −20°C.

We identified the layers of area V1 according to Brodmann's (1909) nomenclature, modified by Lund (1973), in CO and Nissl staining. This system distinguishes four subdivisions of layer 4, namely, 4A, 4B, 4Cα, and 4Cβ. Adjacent sections were used for CO, NeuN, Nissl, and VGluT2 (see Fig. 3E–H). All experimental procedures were approved by the New York University Institutional Animal Use and Care Committee and were conducted in strict compliance with the National Institutes of Health (NIH) guidelines for the care and experimental use of animals in research.

Human brain tissue

Human postmortem tissues from the left hemisphere were obtained from six adults (aged 23–69 years; average 48 years) who died in traffic accidents, and were free of any neurological or psychiatric disorders (kindly supplied by Dr. DeFelipe, Instituto Cajal, CSIC). In all cases, the time between death and tissue processing was between 2 and 3 hours. The brain samples were obtained following the guidelines approved by the Institutional Ethics Committees. Tissue sections from these human brains were used in previous studies (e.g., Inda et al., 2007; Garcia-Marin et al., 2010; Blazquez-Llorca et al., 2010). Upon removal, the brain tissue was immediately fixed in cold 4% PFA in 0.1 M PB, pH 7.4, and after 2 hours, the tissue was cut into small blocks and postfixed in the same fixative for 24–48 hours at 4°C. Parasagittal serial sections (50 μm) were cut by using a vibratome. All sections were immersed in graded sucrose solutions overnight, and were stored in a cryoprotectant solution at −20°C. The tissue was obtained from area 17 (V1) and area 18 (secondary visual area, V2). Nissl-stained sections were used to identify each cortical area. We identified the layers of area V1 according to Brodmann (1909), as described above. The sections were batch-processed for immunocytochemical staining, but due to tissue availability, sections were from the same block (series) but not always adjacent (see Fig. 3A–D).

Antibody characterization

A full list of all antibodies used in this study is presented in Table 1.

The mouse anti-VGluT2 antibody is a recombinant protein from rat VGluT2. In Western blot analysis, it appears as an individual band of ~56 kDa (manufacturer's technical information). The staining pattern corresponded to the pattern described in previous studies using the same monoclonal VGluT2 antibody in the monkey (Hackett and de la Mothe, 2009; Wong and Kaas, 2008, 2009).

The guinea pig anti-VGluT1 antiserum was raised against a synthetic peptide of the C-terminal domain (amino acids 541–560) of rat VGluT1 protein, which revealed a single band of 60 kDa molecular weight on a Western blot (manufacturer's technical information; Boulland et al., 2007). The staining pattern was identical to the data published for humans (Alonso-Nanclares, 2005), and for rats and mice (Alonso-Nanclares et al., 2004; Merchan-Perez et al., 2009).

In Western blots of the mouse cerebral cortex, the monoclonal anti-NeuN antibody recognizes four bands: two of 46–48 kDa and two of 62–68 kDa (Unal-Cevik et al., 2004). The staining pattern was identical to that published for the human cerebral cortex (Inda et al., 2007; Garcia-Marin et al., 2010).

Immunohistochemistry (IHC)

Initially we found that VGluT2 IHC was variable in monkeys. In sections from some animals, we obtained

excellent VGluT2-ir staining by increasing the Triton X-100 concentration to 3%, which enhanced the permeability of the membrane, although in other cases, the staining was less intense even with this high concentration of Triton X-100. In addition, for human tissue, VGluT2-ir staining was only found after antigen retrieval (AR).

In brief, AR protocols are used in IHC to avoid the masking effect of antigens by aldehyde fixation (Shi et al., 1997). AR protocols are based on immersion of the sections in various solutions with different pH and at high temperatures, in order to break the methylene bridges, and expose the highest number of antigenic epitopes (Pileri et al., 1997). A commonly used technique for AR, prior to undertaking IHC, is heating brain sections in citrate buffer (Shi et al., 1991; Suurmeijer and Boon, 1993; Bankfalvi et al., 1994; Jiao et al., 1999). This protocol has been used to enhance the VGluT2 immunoreaction in rats (Varoqui et al., 2002) and mice (Nakamura et al., 2005, 2007), and is used in human and monkey thalamus to show dopamine distribution (Garcia-Cabezas et al., 2007). In the present work, an AR protocol based on Jiao et al. (1999) was used for VGluT2 immunohistochemical detection in both the macaque and human tissue.

After obtaining consistent IHC for human tissue by using AR, we found that variability in the macaque was also eliminated by using AR prior to the IHC protocol, and the intensity matched the best cases we obtained by using 3% Triton X-100. Thus, for all human tissue, AR was used as the first step in VGluT2 processing. For macaque, we either used tissue after Triton X-100 treatment (when there was good staining), or used tissue after preprocessing for AR, as the first step in VGluT2 processing (outlined above for human sections).

Individual floating sections were incubated in a 0.01 M sodium citrate buffer solution (pH 8.0) preheated to 80°C for 15 minutes in a water bath. Sections were cooled down to room temperature for 20 minutes and were subsequently rinsed 3 times in 0.01 M PBS. Sections were then pretreated in 1.66% hydrogen peroxide (H_2O_2) for 15 minutes to remove endogenous peroxidase activity, and subsequently blocked for 2 hours in 0.01 M PBS with 1% bovine serum albumin (BSA). The sections were then incubated overnight at 4°C with mouse anti-VGluT2 antibody (1:4,000; MAB5504, Millipore, Billerica, MA) in 0.01 M PBS with 1% BSA, 0.3% Triton X-100, and 0.05% sodium azide. Sections were rinsed and incubated for 2 hours with biotinylated goat anti-mouse (1:500; BA-9200, Vector, Burlingame, CA). The sections were then incubated for 30 minutes in an avidin–biotin peroxidase complex (Vectastain ABC Elite PK6100, Vector), and finally reacted either with Vector VIP Peroxidase Substrate Kit (SK 4600), which produced an intense violet-colored precipitate, or with 0.05% 3,3′-diaminobenzidine tetrahydrochloride (DAB) (Sigma, St. Louis, MO) and 0.01% hydrogen peroxidase, which produced an intense brown-colored precipitate. After staining, the sections were dehydrated, cleared with xylene, and coverslipped. VGluT2-ir staining patterns after AR were comparable to those previously described for mice and monkeys (Fremeau et al., 2001; Fujiyama et al., 2001, 2003; Boulland et al., 2004; Nahmani and Erisir, 2005; Nakamura et al., 2005; Graziano et al., 2008; Wong and Kaas, 2008, 2009; Hackett and de la Mothe, 2009; Coleman et al., 2010).

In addition, we used NeuN antibody for identifying the V1 layers in macaque and human. In brief, free-floating sections were incubated for 2 hours in 0.01 M PBS with 1% BSA, and then were incubated overnight at 4°C with the primary mouse anti-NeuN (1:2,000; Millipore). The following day, they were rinsed and incubated for 2 hours with biotinylated goat anti-mouse IgG (1:500; Vector). Antibody binding was detected with an ABC immunoperoxidase kit and visualized either with the VIP Peroxidase Substrate Kit or DAB. After staining, the sections were dehydrated, cleared with xylene, and coverslipped.

Controls for the secondary antibodies were administered in all the IHC procedures, either by replacing the primary antibody with preimmune goat serum in some sections, by omitting the secondary antibody, or by replacing it with an incompatible secondary antibody. No significant staining was detected under these control conditions.

Fluorescence immunohistochemistry

To determine whether VGluT2-ir puncta colocalized with VGluT1-ir puncta, dual-fluorescence immunohistochemistry was used. Free-floating sections were incubated for 1 hour in 0.01 M PBS with 0.3% Triton-X and 3% normal goat serum (Vector). For this procedure, this concentration of Triton-X was sufficient to give excellent fluorescence images. The sections were then incubated overnight at 4°C with a combination of antibodies: mouse anti-VGluT2 (1:4,000) and guinea pig anti-VGluT1 (1:5,000; Millipore). The following day, the sections were rinsed and incubated for 2 hours with biotinylated goat anti-guinea pig Ig (1:500; Vector). The sections were then incubated for 2 hours at room temperature with streptavidin coupled to Alexa Fluor 594 (1:1,000; Molecular Probes, Eugene, OR) and with Alexa Fluor goat-anti mouse 488 (1:2,000; Molecular Probes). After three rinses in 0.01 M PBS, the sections were treated with Autofluorescence Eliminator Reagent (Chemicon, Temecula, CA) to reduce or eliminate lipofucsin-like autofluorescence without adversely affecting any other fluorescent label in the sections. The sections were rinsed three times in 0.01 M PBS and mounted in ProLong Gold Antifade Reagent (Invitrogen, Carlsbad, CA).

Confocal images (physical size 81.91 × 81.91 μm, logical size 2,048 × 2,048 pixels) were obtained by using a Leica SP5 confocal laser scanning microscope (Leica Microsystems, Wetzlar, Germany), with a 63× magnification oil-immersion lens (NA 1.40, refraction index 1.52), using an optical zoom factor of 3.0. Six non-overlapping images were obtained from layers 4A and 4Cβ from six animals.

Cytochrome oxidase histochemistry

Adjacent sections to those processed for IHC were reacted for CO, both in macaque and human tissue (Wong-Riley, 1979; Horton and Hubel, 1981; Horton et al., 1990). Free-floating sections were pretreated in 1% H_2O_2 for 30 minutes. The sections were incubated in a solution containing 0.01 M PBS, 4.5% sucrose, 0.033% cytochome C, 0.055% DAB, and 0.02% catalase for 14 hours at 37°C. Reaction was stopped with 0.01 M PBS rinses when the cortical layers 4A and 4C, and the patches in layers 2 and 3 were visible. In some sections, layer 4C was visible as early as 1 hour, layer 4A appeared at 2 hours, and layers 2 and 3 patches were recognized at 3 hours. After 4 hours of incubation, all the previous regions were darker and Meynert cells became visible in layer 6. Our incubation time of 14 hours allowed us to obtain distinct contrast between the layers but without increasing the background. After several rinses, the sections were dehydrated, cleared with xylene, and coverslipped.

Measurement of the proportion of layers 4A and 4B containing VGluT2-ir puncta

To estimate the proportion of layer 4B that showed VGlut2-ir puncta, we measured the regional extent of VGluT2-ir puncta in two human and two macaque sections at 200× magnification. Layer 4B was defined in the VGluT2 sections by the boundaries of layer 4A and 4C. First, for a fixed length of 4B (~7 mm), each region that had discernible puncta was delineated. The linear extent of these regions was summed and expressed as a percent of the total length studied. In addition, the vertical extent of layer 4B was measured along the same fixed length of 4B that was examined for VGluT2. At 0.5-mm intervals, the relative vertical extent of 4B within layer 4 was measured by determining the extent of 4B from the layer 4A/4B border to the 4B/4C border as a proportion of the total vertical extent from the 4A/4B border to the 4C/5 border normal to the surface (Hawken et al., 1988). We determined the relative extent of 4B over the 4B + 4C distance rather than the absolute extent of 4B within the total cortical depth to minimize variability due to the angle of sectioning. No shrinkage correction was taken into account. The relative extent of human layer 4A that contained VGluT2-ir puncta was estimated by using the same methodology described above for layer 4B.

Minicolumn measurement

The high density of VGluT2-ir puncta in layer 4C gives a very clear picture of the minicolumnar organization of the visual cortex (see Fig. 2A,E). We used images obtained at 200× magnification from sections from each of three humans ($n = 29$, $n = 16$, and $n=22$ for the three humans; total number of minicolumns = 67) and three macaques ($n = 35$, $n = 35$, and $n = 29$ for the three macaques; total number of minicolumns = 99), to measure the lateral minicolumn dimensions. Minicolumns were defined by a central core area that contains the majority of the neurons, apical dendrites, and myelinated afferent fibers. This central core is flanked on either side by cell-poor areas (peripheral neuropil space) that are rich in unmyelinated axon fibers, dendritic arborizations, and synapses (Jones and Burton, 1974; Szentagothai, 1978; Seldon, 1981, 1982; Ong and Garey, 1990; Peters and Payne, 1993; Peters and Sethares, 1996; Mountcastle, 1997). Some authors have referred to these peripheral neuropil spaces as microzones (DeFelipe and Jones, 1991). Following Casanova et al. (2009) we used the term *core width* for the region relatively free of VGluT2-ir puncta that contains the majority of the neuronal cell bodies (see Fig. 2A,E); and *minicolumnar width* for the average distance from center to center of two adjacent peripheral neuropil spaces that are VGluT2-ir dense.

Image processing

To generate the figures, images were captured with an Olympus Microfire digital Camera attached to an Olympus BX51 light microscope. Adobe Photoshop CS3 software (Adobe Systems, San Jose, CA) was used to adjust the images for brightness and contrast, and to generate the figure plates. Images were not altered in any way, e.g., by removing or adding image details. Minimum intensity Z projections of the light microscopic images were obtained by using ImageJ software (NIH).

RESULTS

We studied the distribution pattern of VGluT2-ir puncta in human and macaque V1 cortex to determinate if the pattern matches the LGN thalamic afferent terminal distributions, and to compare the pattern between species. Previous studies have shown that VGluT2-ir puncta in V1 colocalize to the afferent terminations from the LGN in ferret (Nahmani and Erisir, 2005) and mouse (Coleman et al., 2010). VGluT2 has been used as a marker of thalamic terminations in the gray squirrel (Wong and Kaas,

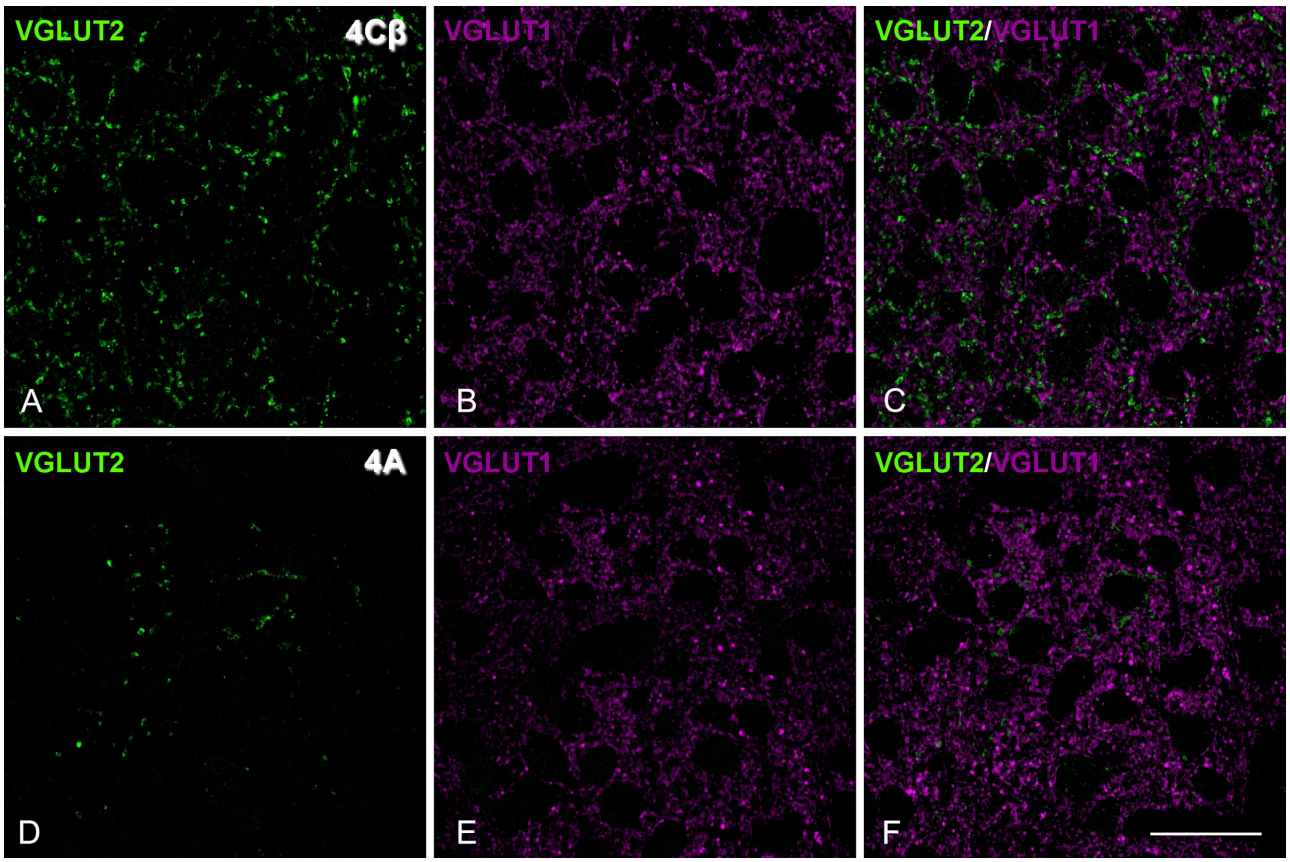

Figure 1. No colocalization in the dual labeling for VGluT1 and VGluT2 in macaque V1, layer 4Cβ (A–C) and 4A (D–F). **A,D**: Single confocal optical sections of VGluT2-immunoreactive (-ir) puncta (green). **B,E**: Single confocal optical sections of VGluT1-ir puncta (magenta). **C,F**: Merge of both channels. Scale bar = 22 μm in F (applies to A–F).

2008) and tree shrew (Wong and Kaas, 2009). Initially, we established that VGluT2-ir puncta were labeled independently of VGluT1-ir puncta in macaque. In the neuropil of layer 4Cβ, where there is the highest density of VGluT2-ir puncta (Fig. 1A), there is also a high density of VGluT1-ir puncta (Fig. 1B) in confocal images of the same section. When the images were merged (Fig. 1C), there were very few dual-labeled puncta (<1%: VGluT2-ir puncta = 1,923, VGluT1-ir puncta = 6,229, VGluT1 and VGluT2 = 67), confirming that in the primate V1, as in the mouse and in the ferret, the two populations are essentially independent. Similar analysis of the VGluT2-ir puncta in layer 4A (Fig. 1D) compared with VGluT1-ir puncta (Fig. 1E) yielded no dual labeling (Fig. 1F).

Distribution pattern of VGluT2-ir puncta in human V1

VGluT2-ir puncta showed a laminar-specific pattern in V1 (Figs. 2A, 3D), with a clear boundary between V1 and V2 (Fig. 2B, dashed line) where the VGluT2-ir was dense in layer 4 of V1, and the distinct laminar pattern ended abruptly at the V1/V2 border. In V1, VGluT2-ir puncta were found in layers 1, 4A, 4C, and 6, and as patches in layers 2 and 3, with the highest density in 4C.

Granular layers

Within layer 4C, the highest VGluT2-ir density was found in 4Cβ. There was a reduction in the puncta density between 4Cβ and 4Cα (Fig. 2E). At the lower boundary of layer 4, there was a very clear change in VGluT2-ir density between layer 4Cβ and 5 (Fig. 2A,E). At the 4Cα/4B boundary, there was also a large reduction in puncta density, but the transition was not as uniform as found at the lower boundary, undulating vertically over about 25–50 μm (Fig. 2E). In the CO staining, 4C was also clearly observed as a wide band of high intensity (Fig. 3C).

It has been suggested that the gradual change in CO density from 4C to 4B in humans may also correspond to a gradual reduction in the density of LGN afferent terminations (Preuss et al., 1999; Preuss and Coleman, 2002). This would mean that there should be an observable change in density of puncta in layer 4B. Although we observed a relatively abrupt change in VGluT2-ir between

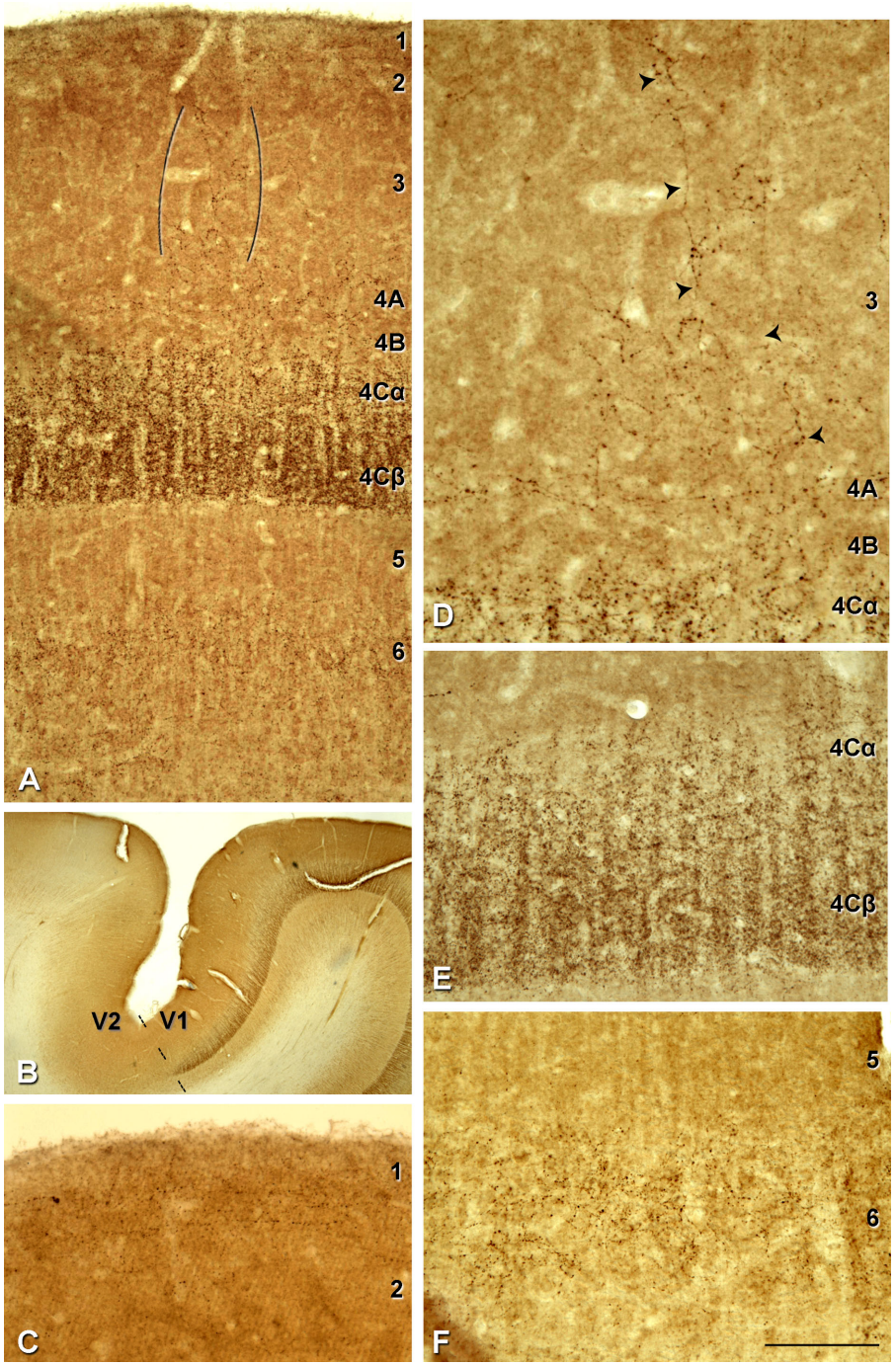

Figure 2. VGluT2-ir pattern in human V1. **A**: Immunostaining in layers 1, 2/3, 4A, 4Cα, 4Cβ and 6. VGluT2-ir puncta in layer 3 (indicated between brackets). **B**: V1/V2 border (dashed line) stained for VGluT2. There is a very clear laminar pattern of VGluT2-ir in V1 that ends abruptly at the V2 border. **C**: VGluT2-ir puncta in layer 1 prominently found in the upper half of the layer. **D**: Higher magnification of VGluT2-ir puncta fibrous pattern in layer 3 (indicated by the arrowheads). **E**: Higher magnification of layers 4Cα and 4Cβ; due to the high density of VGluT2-ir puncta in these layers cortical minicolumns are clearly observed. **F**: Higher magnification of VGluT2-ir puncta in layer 6. Scale bar in F = 200 μm for A; 2,150 μm for B; 145 μm for C,E,F; 110 μm for D.

layer 4Cβ and 4B at the level of the minicolumns, there were also a few isolated regions of layer 4B that had detectable VGluT2-ir puncta, and these regions appeared to spread up into the supragranular layers (Fig. 4). To estimate the proportion of layer 4B that showed VGlut2-ir, we determined the regions that had a discernible density of puncta. Over a length of 7 mm in one case (M17), we found only 8% of the length of 4B had puncta, and almost all of these were in the one region shown in Figure 4. Even in this region, the density was very low compared

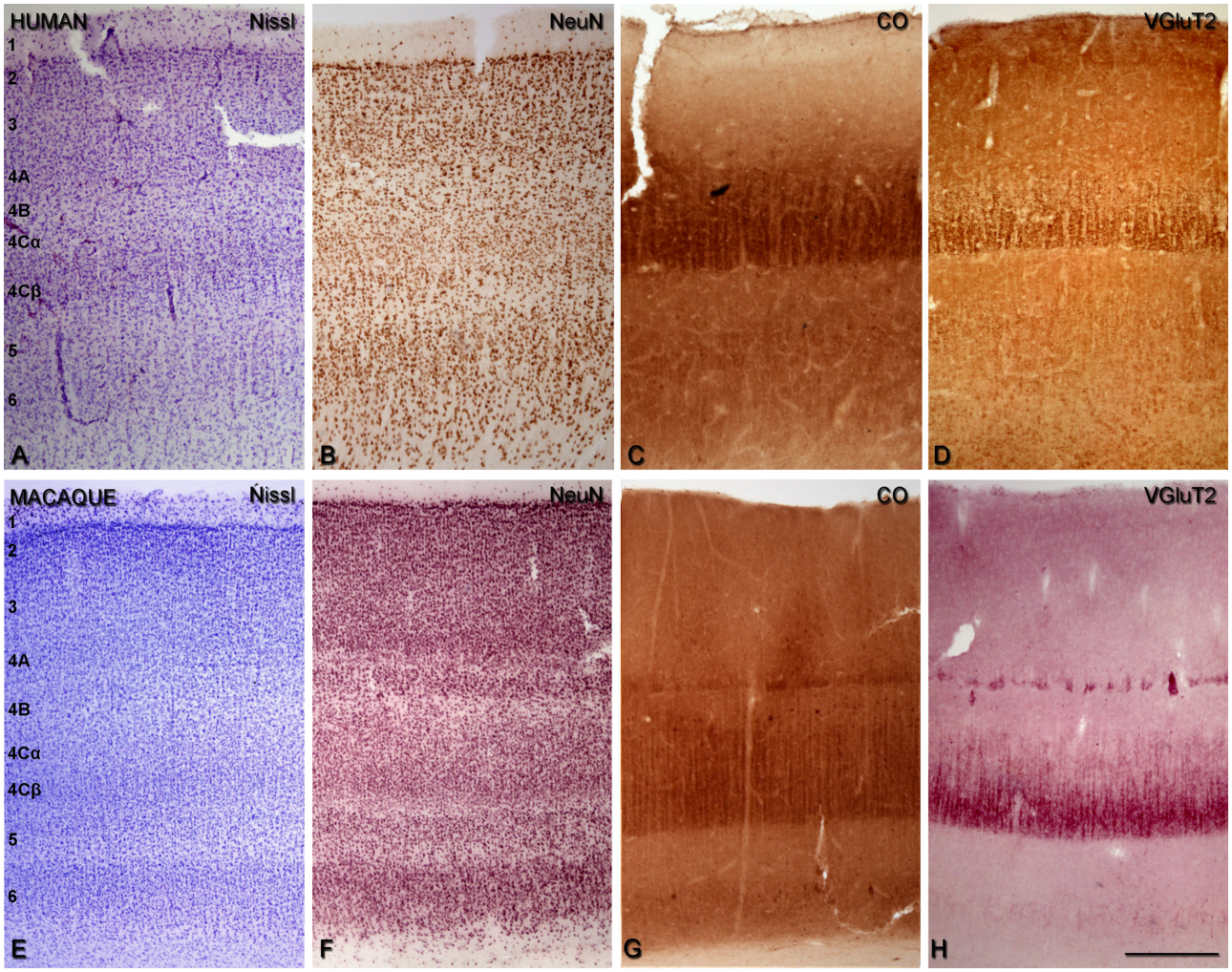

Figure 3. Comparison of the cellular and laminar organization of V1 in human (A–D) and macaque sections (E–H). Nissl staining (**A,E**), NeuN-ir (**B,F**), cytochrome oxidase (CO) staining (**C,G**), and VGluT2-ir (**D,H**). In macaque, sections were adjacent. Scale bar = 400 μm in H (applies to A–H).

with 4C (compare density in Fig. 4 [layer 4B] with Fig. 2E [layer 4C]). In a second case (M16), similar analysis showed that 2.5% of 4B had discernible puncta. Our analysis suggests that the presence of VGluT2-ir puncta in 4B is rare. The vertical extent of layer 4B was another measure that we obtained by using the VGluT2 distribution. The relative extent of 4B within layer 4 was 19% (ratio 4B/(4B + 4C) = 0.2 ± 0.04 and 0.18 ± 0.05; n = 14, and n = 15, for M17 and M16, respectively) for two human cortices, compared with 25.5% (ratio 4B/(4B + 4C) = 0.27 ± 0.03 and 0.24 ± 0.03; n = 16, and n = 14, for M607 and OB7, respectively) for macaque (all values are mean ± SD). Thus, based on these measurements, there is a decrease in the extent of layer 4B from macaque to human.

Human layer 4A has been difficult to characterize because it is seen as a narrow band (~100 μm wide) of densely packed small cells in either Nissl (Brodmann, 1909) or NeuN (Fig. 3A,B) stained sections. In addition, it does not stand out as a distinct narrow band as it does in macaque, when tissue is stained for CO (compare Fig. 3C and G). The distribution of VGluT2-ir in this region is patchy (Figs. 3D, 4) although it does not stand out as the characteristic honeycomb pattern that is found in macaque (Figs. 5B, 6). Nonetheless, there are regions of increased density that run horizontally above the upper boundary of 4B (Fig. 4). In a similar analysis as described for layer 4B above, we found that 48% and 49% of layer 4A (in M17 and M16, respectively) was occupied by VGluT2-ir puncta (Fig. 4). The puncta in this region appear as horizontal bands. When VGluT2-ir patches in 4A do not extend into layer 3, they do not appear to extend across the full vertical extent of 4A as defined in the Nissl sections.

The high density of VGluT2-ir puncta in layer 4C gives a very clear picture of the minicolumnar organization of the visual cortex. We have used the term *core width* for the

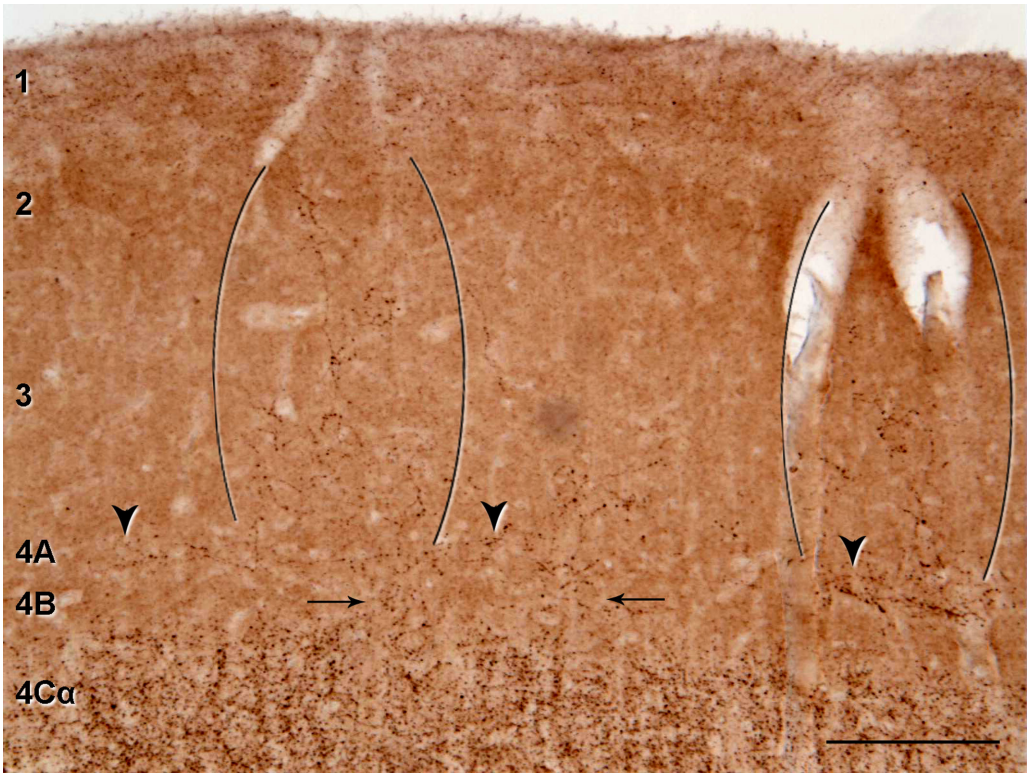

Figure 4. VGluT2-ir puncta in supragranular and granular layers of human V1. **A**: Low-power photomicrograph illustrating the repetitive pattern of VGluT2-ir puncta in layers 2 and 3. There are two patches of puncta (indicated between two sets of brackets), that are separated by about 600 μm. Some VGluT2-ir puncta are also present in layer 4B (arrows) and patchy staining of VGluT2-ir puncta in layer 4A (arrowheads). Scale bar = 200 μm.

region relatively free of VGluT2-ir puncta that contains the majority of the neuron cell bodies (Fig. 2A,E); and *minicolumnar width* for the average distance from center to center of two adjacent peripheral neuropil spaces that are VGluT2-ir dense. We found that the minicolumnar width was 24.7 ± 5 μm (mean ± SD; $n = 67$), and the core width was 11.9 ± 3 μm (mean ± SD; $n = 67$). Thus, neurons in the minicolumns occupied the central core (~12 μm) and are bordered by 6.4 μm of VGluT2-ir puncta.

Supragranular layers

There were distinct VGluT2-ir puncta in layer 1 (Fig. 2C), especially in the upper half of this region, and patches in layers 2 and 3 (Figs. 2A,D, 4). It is the first time that putative geniculate afferent terminals have been described in human V1 outside layers 4 and 6 (Miklossy, 1992). We compiled a histogram of the center-to-center distance between neighboring high-density VGluT2-ir regions in layers 2 and 3; in the histogram the first peak was centered at about 0.8–1.0 mm. Furthermore, some clusters of puncta within a patch often showed a pattern suggesting that they originate from a single fiber (Fig. 2D, arrowheads), rising near layer 4A, and coursing up to layer 2. Presumably, the puncta in each patch are derived from a number of ascending fibers. A clear patchy staining was not observed in layers 2 and 3 for CO histochemistry, although in certain regions, some faint patches were observed; probably a longer incubation time for CO is needed for more robust CO staining.

Infragranular layers

In the infragranular cortical layers, there was a very clear difference in distribution of the VGluT2-ir puncta. Layer 6 had a moderate density of terminals that extended along the layer; there were no regions without puncta in the horizontal direction (Fig. 2A,F). In layer 5, where there were few VGluT2-ir puncta, there was a sharp transition between 4C and 5A at the upper border (Fig. 2A,E), and a discernible border between lower layer 5 and upper 6 (Fig. 2F). Within layer 6, where the distribution was not uniform, there was a higher density in the middle region of layer 6, with a sparser distribution in the upper and lower portions (Fig. 2F). There was an indication of periodicities in layer 6 (Fig. 2F). The pattern in layer 6 is described in more detail later in the macaque sections. With the CO histochemistry, we could not discern the differential density or periodicity within layer 6 (Fig. 3C).

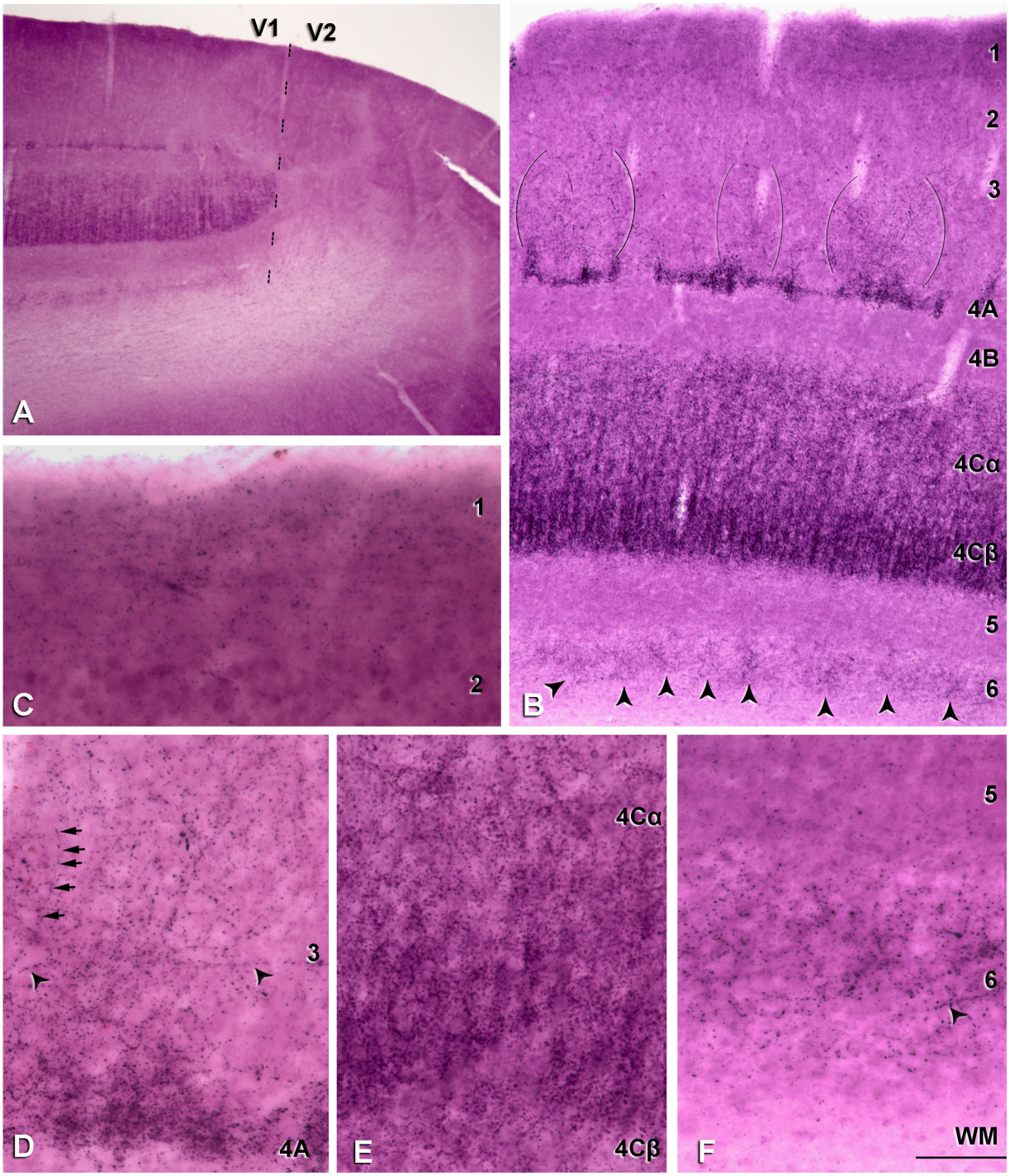

Figure 5. Layer-specific distribution of VGluT2-ir puncta in macaque V1. **A**: Low-power photomicrograph of a section at the V1/V2 border, indicated by a dashed line. There is a very clear laminar pattern of VGluT2-ir in V1 that ends abruptly at the V2 border. **B**: VGluT2-ir pattern through the depth of V1 shows immunostaining in layers 1, 2/3, 4A, 4Cα, 4Cβ and 6. VGluT2-ir puncta in layers 2 and 3 (indicated between the three sets of brackets) shows repetitive patches that are approximately 400 μm apart. In layer 6, there is a patchy distribution with regions of higher density (arrowheads), separated by regions of lower density. The scale of the horizontal separation of the patches is about 50 μm, greater than the width of the minicolumns (~20 μm) that are seen in layer 4C and narrower than the patches in layers 2 and 3 seen in A. **C**: VGluT2-ir puncta of layer 1 are predominantly found in the upper half of the layer. **D**: Higher magnification of one VGluT2-ir dense region in layers 2 and 3; most of the fibers seem to derive from layer 4A and rise vertically to end in layers 2 and 3. Some horizontal (arrowheads) and vertical beaded fibers moving toward layer 1 (arrows) could also be observed. The density of puncta in some regions of layer 4A was high, similar to the density in layer 4C (see E). **E**: Layers 4Cα and 4Cβ have the highest density of VGluT2 puncta in V1. Cortical minicolumns are clearly observed, and run vertically. **F**: Layer 6 shows a moderately dense puncta distribution, whereas in layer 5 the distribution is sparse. Horizontal beaded profiles were also observed (arrowhead), which suggests that single axons are making multiple contacts. WM, white matter. Scale bar in F = 400 μm for A; 220 μm for B; 75 μm for C; 65 μm for D–F.

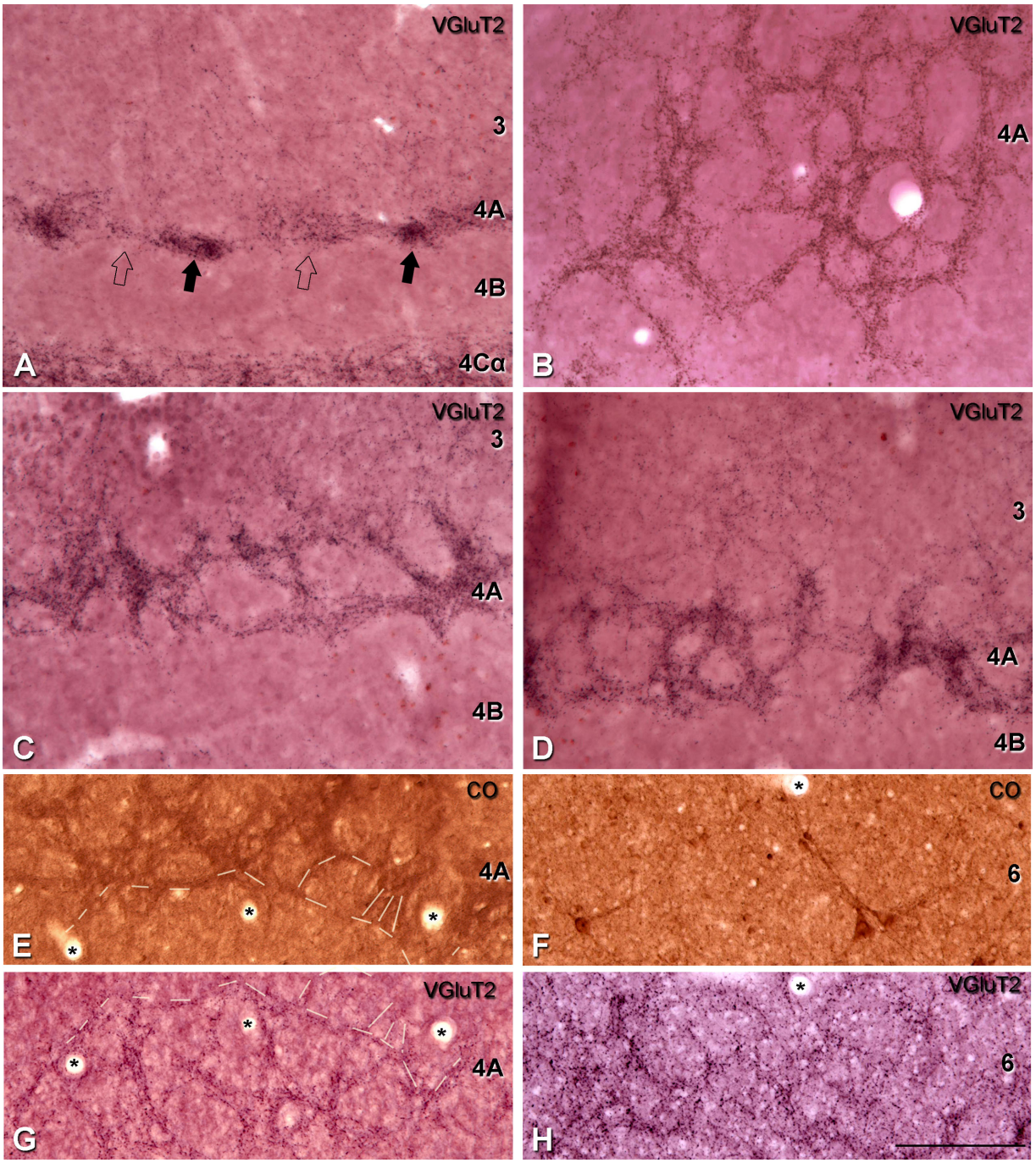

Figure 6. The organization of VGluT2 puncta in layer 4A and 6 of macaque. Sections cut either parasagittally, horizontally, or obliquely and immunoreacted for VGluT2 show intense staining with a structural pattern resembling the honeycomb characteristic seen in cytochrome oxidase (CO) (Horton, 1984; Fitzpatrick et al., 1985) and in transneuronal transport to V1 after labeling one eye (Horton, 1984). **A**: Parasagittal section of layer 4A showed very high density areas of VGluT2 (filled arrow) adjacent to areas with lower density (open arrow). **B**: Horizontal section of layer 4A showed a continuous network of VGluT2. **C,D**: Oblique planes section through layer 4A showed only one layer of the honeycomb arrangement, where the puncta dense regions are about 30–40 μm wide surrounding puncta-sparse regions. **E,G**: Adjacent horizontal sections processed for VGluT2 (G) and CO (E), showed the characteristic honeycomb pattern in layer 4A and it is clearly continued from one section to the next (dashed lines). **F,H**: Adjacent horizontal sections processed for VGluT2 (H) and CO (F) through layer 6 showed a clear annular pattern of VGluT2-ir puncta. The adjacent section stained for CO did not show any of the patterning seen with VGluT2 although the giant Meynert cells were clearly visible. (*), blood vessels were used to align adjacent sections. Scale bar in H = 150 μm for A–D and E–H.

Distribution pattern of VGluT2-ir puncta in macaque V1

We studied the distribution pattern of VGluT2-ir puncta to determine the degree of correspondence with the established distribution of LGN afferents in macaque V1. VGluT2-ir terminals show a laminar-specific pattern in V1 (Figs. 3H, 5B). Qualitatively, the pattern shown in Figures 3H and 5B closely matches the pattern that would be generated from combining the results from tracing studies (Hendrickson et al., 1978; Fitzpatrick et al., 1983; Blasdel and Lund, 1983; Freund et al., 1989; Casagrande et al., 2007). In general, VGluT2-ir terminals showed a laminar-specific pattern in V1 (Figs. 3H, 5B), with the highest density in layers 1, 4C, and 6, and in patches in 2/3. The VGluT2-ir showed a clear demarcation of the V1/V2 boundary (Fig. 5A).

Granular layers

There was a high density of VGluT2-ir puncta in layer 4C with very clear divisions between 4Cα and 4B, and also between 4Cβ and 5 (Fig. 5B). Within layer 4C, there was a higher density of puncta in the lower half corresponding to layer 4Cβ, than in the upper half of 4C, 4Cα (Fig. 5B,E).

Layer 4B in macaque was virtually devoid of VGluT2-ir puncta (Figs. 5B, 6A), although rarely, it was possible to see some VGluT2-ir puncta crossing this layer. As reported above, the relative extent of 4B was about 25% the width of 4C when defined by VGluT2-ir puncta.

Layer 4A (Fig. 6A–D) showed a high density of VGluT2-ir puncta with a structural pattern resembling the honeycomb characteristic of this layer when stained for CO histochemistry (Horton, 1984). Depending on the plane of section, different puncta patterns were observed. In the parasagittal plane, areas with very high VGluT2-ir puncta density (Fig. 6A, filled arrows) were seen adjacent to areas with lower puncta density (Fig. 6A, open arrows). In horizontal sections, a continuous clustered puncta network of VGluT2 was clearly observed (Fig. 6B). In an oblique plane of section, only one layer of this honeycomb network was observed (Fig. 6C,D).

Furthermore, layer 4C in macaque showed a high density of VGluT2-ir puncta, which allowed us to obtain measurements of minicolumnar organization. We found that the minicolumnar width (spacing) was 18.0 ± 3.4 μm (mean ± SD; $n = 99$), and the core width was 8.9 ± 2.6 μm (mean ± SD; $n = 99$). Neurons in the minicolumns of macaques occupied the central core (~9 μm) and were bordered by 4.5 μm of VGluT2-ir puncta.

Supragranular layers

There were VGluT2-ir puncta in layer 1 (Fig. 5C) and patches in layers 2 and 3, (Fig. 5B). In layers 2 and 3, the period of the pattern of higher density VGluT2-ir puncta patches was approximately 400 μm, measured as the center-to-center distance between adjacent high-density VGluT2-ir regions (Fig. 5B). In a later section of the Results, we show that the periodicity of the VGluT2-ir patches matches the periodicity of CO patches observed in layers 2 and 3 (Wong-Riley, 1979). Within the denser VGluT2-ir regions of layer 3, there were often single radiating sequences of dark staining spots (Figs. 5D) that may correspond to boutons of single afferent fibers (Casagrande et al., 2007). Within layer 1, there was a preponderance of VGluT2-ir that was especially noticeable in the upper half of layer 1 (Fig. 5C). Sometimes it was possible to see that these fibers were collaterals coming from the VGluT2-ir patches in layers 2 and 3.

Infragranular layers

Layer 6 showed VGluT2-ir puncta particularly in the upper half of the layer where it was possible to observe a patchy pattern (Fig. 5B, arrowheads, F). The middle to lower region of the upper half of layer 6 contained areas with the highest density of puncta (Fig. 5B). Occasionally, puncta were observed in the upper border region of layer 6, but in general, the upper region showed a lower density of VGluT2 than the middle region (Fig. 5B). The nature of this pattern in layer 6 is analyzed below. Finally, layer 5 was virtually devoid of VGluT2-ir puncta (Fig. 5B), although occasionally, it was possible to see some VGluT2-ir puncta crossing the layer.

VGluT2-ir IHC versus CO histochemistry

To further analyze the distinctness of VGluT2 labeling, we compared layers 2 and 3, and 4A and 6 in adjacent sections stained for VGluT2 and CO. To determine the correspondence between the periodicity of the VGluT2-ir puncta density and CO patches in layers 2 and 3, we processed adjacent parasagittal and horizontal sections for VGluT2 and CO. In both cases of parasagittal (Fig. 7) and horizontal sections (data not shown), VGluT2-ir puncta in layers 2 and 3 of one section (Fig. 7A,C) were found in alignment with CO patches in an adjacent section (Figs. 7B,D). The repetitive CO patches were clearly visible at lower magnification (Fig. 7B); however, it was not possible to clearly view the VGluT2-ir puncta at low magnification (Fig. 7A). When higher magnification was used to observe the VGluT2-ir puncta in layers 2 and 3 (Fig. 7C), we found that they colocalized with the CO patches (Fig. 7D).

In layer 4A, adjacent horizontal sections were processed for VGluT2 and CO. The characteristic honeycomb pattern was observed and clearly continued from one section to the next (Fig. 6E,G). In VGluT2 IHC, individual VGluT2-ir puncta form the edges of the honeycomb and the VGluT2-ir puncta provide the overall pattern of terminal density, clearly showing that there are few if any

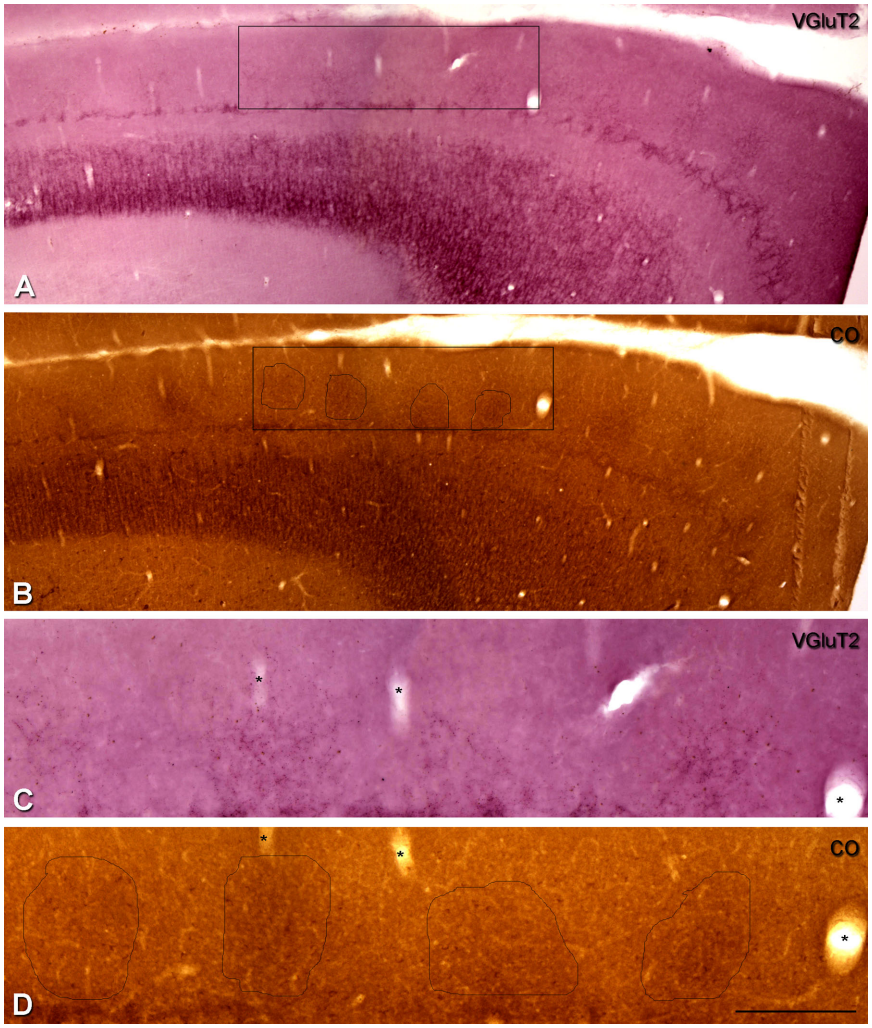

Figure 7. Comparison of the patches of higher density of VGluT2-ir puncta in layers 2 and 3 with the distribution of CO-rich patches in macaque V1. **A,B**: Adjacent parasagittal sections through the depth of V1 show sections processed for VGluT2 immunohistochemistry (A) and cytochrome oxidase (B). The regular pattern of CO-rich patches is seen in layers 2 and 3 in B. **C,D**: To compare the CO-rich patches in layers 2 and 3, four patches were selected within the outline of the box so that at higher magnification the VGluT2-ir patches in layers 2 and 3 can be seen to correspond with the CO-rich patches. (*), Blood vessels were used to align the adjacent sections. Scale bar in D = 600 μm for A,B; 200 μm for C,D.

puncta in the non-border regions. The continuous staining observed in sections processed for CO gives the outline of the honeycomb but does not indicate whether there are terminals in the lower density regions.

To determine the nature of the arrangement in layer 6 and to estimate the extent of the pattern in depth, a series of horizontal sections was prepared from additional blocks from three animals. We found that VGluT2-ir puncta formed a clear, annular pattern of puncta density (Fig. 6H). This highest density of puncta was found in the upper-middle of layer 6, covering an extent of about 120 μm. Above and underneath this higher density region, we found an area with middle density of puncta (~60 μm in each side). Close to layer 5 and white matter, the VGluT2-ir puncta disappeared. In the middle region, the diameter of the annular pattern ranged from small rings of 30–100 μm. The edges of the rings showed high density of puncta, surrounding areas with a low density of VGluT2-ir puncta or, in some instances, without puncta. The adjacent sections stained for CO did not show any of the pattern seen with VGlutT2, although the giant Meynert cells were clearly visible (Fig. 6F).

VGluT2-ir puncta in V2

When sections reacted for VGluT2 were viewed at low power, there was a clear boundary between V1 and V2 (Fig. 2B, dashed line) where the distinct laminar pattern of VGluT2-ir puncta in V1 ended abruptly at the V1/V2 border. However, within V2, there was no clear laminar pattern, as found in V1, when observed at low magnification neither in human nor macaque (Figs. 5A, 8B,C). At

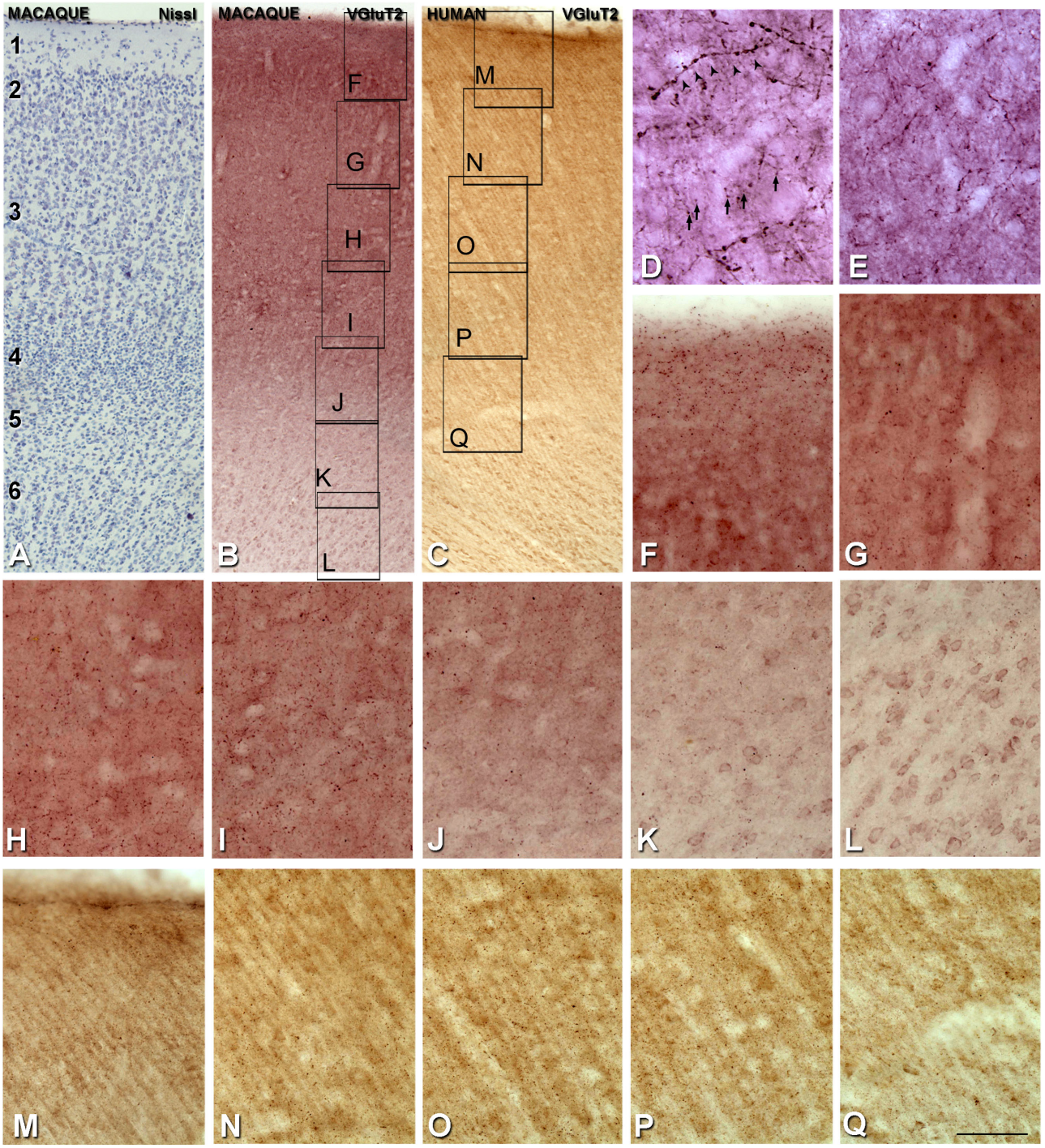

Figure 8. Distribution of VGluT2 in V2 of macaque and human. **A**: Nissl-stained section of macaque V2. **B**: Adjacent section stained for VGluT2, **C**: Human V2 stained for VGluT2. **D**: VGluT2-ir puncta in layer 4 of V2 (arrows), close to the V1/V2 border. Some fibers (arrowheads) are large and appear to come from axons with branches in V1 and V2. **E**: VGluT2-ir puncta in layer 4 of V2. **F–L**: Higher magnification images from B, showing the distribution of VGluT2-ir puncta throughout the depth of V2, from layer 1 to 6 in macaque. **M–Q**: Higher magnification images from C, showing the distribution of VGluT2-ir puncta through the depth of V2, from layer 1 to 6 in human. Scale bar in Q = 180 μm for A,B; 30 μm for D,E; 80 μm for F–Q.

higher magnification (Fig. 8D–Q), VGluT2-ir puncta were observed preferentially in lower layer 3, in upper layer 4, and in layer 1 (in macaque) of V2. Layers 2 and 5 were less dense than layers 1, 3, and 4, whereas in layer 6 the density was very low. Qualitatively, the size of the VGluT2-ir puncta in layers 3 and 4 of V2 were smaller than the majority of puncta in layer 4C of V1 (Fig. 8D,E). Close to the V1/V2 border, it was possible to observe

small layer 3/4 VGluT2-ir puncta in V2 (Fig. 8D, arrows), similar in size to those outside the border region (Fig. 8E). In addition, in the same region we found large VGluT2-ir puncta (Fig. 8D, arrowheads), probably coming from axons arborizing in V1 and V2, which are larger than VGluT2-ir puncta in V2.

DISCUSSION

In this study, we established that there was a close correspondence between the known pattern of LGN afferents to V1 in the macaque and the distribution of VGluT2-ir puncta. In all the layers of V1, we found that VGluT2 provided a reliable marker for the known pattern of LGN afferent terminals. Utilizing this equivalence between VGluT2 and the LGN afferents, we have studied the distribution of VGluT2-ir in human V1 and ascribe their distribution to putative LGN afferent terminations in human V1. Qualitatively, the distribution of VGluT2-ir in macaque and human V1 is similar in layer 4C. Layer 6 in both macaque and human had VGluT2-ir puncta that were more concentrated in the middle region of the layer where there is a periodic annular pattern that is not observed using CO histochemistry. We also found pronounced differences between human and macaque. In layer 4A of the macaque, there was the characteristic periodic pattern in parasagittal sections that appeared as a honeycomb pattern in horizontal sections, whereas in human, there were sparse horizontally organized patches without the periodicity or density characteristic of macaque. In layers 2 and 3 of the macaque, there was a stable periodic pattern 400 μm between VGluT2-ir patches. In human, VGluT2-ir patches were separated by 800–1,000 μm. In the following sections, we will discuss the correspondence between VGluT2 and other methods of marking afferent terminals in the macaque, as this is a key factor in determining whether VGluT2 is localized in thalamic afferent terminals, predominantly from the LGN for V1 and pulvinar for V2. We will then go on to discuss the distribution of VGluT2-ir puncta in human cortex in more detail.

VGluT2-IHC: a marker for thalamic afferent terminals in macaque visual cortex

In ferret (Nahmani and Erisir, 2005) and in mouse (Coleman et al., 2010), VGluT2 is localized to the terminals of LGN afferents in the visual cortex. In tree shrew and gray squirrel, VGluT2 has been suggested as a putative marker for thalamic afferents in V1 (Wong and Kaas, 2008, 2009). In order to successfully apply IHC for VGluT2 in macaque and human, an AR protocol is a critical step. Without the AR step preceding the IHC, false negatives or partial results are obtained, especially in V2 where a close analysis is needed to observe the presence of VGluT2-ir puncta. The differential laminar distribution of VGluT2-ir puncta in our current study of V1 closely matches the known distribution of thalamic inputs from the LGN to V1. These results suggest that the VGluT2-ir puncta in V1 labels the LGN afferent terminals; the details are discussed below.

The highest density of LGN thalamic afferents is seen in layer 4C, which is the principal recipient zone of thalamic afferents in V1 (Hubel and Wiesel, 1969, 1972; Garey and Powell, 1971; Lund, 1973; Wiesel et al., 1974). There is a high density of VGluT2-ir puncta in layer 4C that corresponds closely to the distribution found after transneuronal anterograde labeling from the retina (Hubel et al., 1977) or LGN (Hubel and Wiesel, 1972; Hendrickson et al., 1978). Layer 4Cβ has a higher density of VGluT-ir puncta than layer 4Cα, which is evident even in the low-power micrographs. There are sharply defined borders in VGluT2-ir puncta density between layers 4B and 4Cα, and between layers 4Cβ and 5. These borders match those of the higher density of CO staining that is also used to define the upper and lower transitions of layer 4C (Peters, 1994). At a finer scale in layer 4Cβ, VGluT2-ir puncta show a periodic pattern of 18.0 μm (column width) and 9.1 μm (core width), which is similar to the data obtained by Casanova et al. (2009) using Nissl staining to measure the minicolumn dimensions in layer 4 of the macaque V1 (16.6 and 9.4 μm, column width and core width, respectively).

DeFelipe and Jones (1991) demonstrated that PV-ir asymmetric synapses from the LGN terminate predominantly in layer 4 of macaque V1, in series of microzones in the neuropil, separated by similar neuropil regions without thalamocortical synapses. The shape and size of these microzones are irregular, but range between 10 and 50 μm in diameter. These microzones of PV-ir asymmetric synapses could correspond to the VGluT2-ir puncta observed surrounding the core of the minicolumns. In addition, Peters and Sethares (1991b) studied the cortical organization of macaque V1 and found clusters of apical dendrites to have an average center-to-center spacing of about 30 μm, a result that exceeds our estimation. The different methodology used in the Peters and Sethares study could explain the discrepancy. The used on antibody that labels microtuble-associated protein 2 (MAP2) within the perikarya and dendrites of neurons, whereas we used VGluT2, which labels the putative thalamic afferent terminals.

Layer 4A shows a characteristic repetitive honeycomb pattern when sections are stained for CO (e.g., Carroll and Wong-Riley, 1984; Horton, 1984; Fitzpatrick et al., 1985). The honeycomb pattern is formed by axon terminals from the lateral geniculate (Hendrickson et al., 1978;

Horton et al., 1984; Hendry and Yoshioka, 1994; Ding and Casagrande, 1997; Casagrande et al., 2007). In fact, layer 4A is composed of a group of pyramidal neurons and apical dendrites that are surrounded by a cell-sparse lattice pattern (Peters and Sethares, 1991a,b). This lattice is clearly visible in all the sections processed for VGluT2, confirming the glutamatergic nature of these afferents presumably arising from the parvocellular or koniocellular layers of the LGN. These terminals probably correspond to the parvalbumin-ir large asymmetrical synapses identified in layer 4A using EM (Peters and Sethares, 1991a). Interestingly, the honeycomb structure characteristic of layer 4A presents a clear demarcation of the putative LGN afferent termination with VGluT2 staining.

One of the striking features of striate cortex in many primate species is the regular periodic pattern of CO density in layers 2 and 3, CO-rich patches. These patches are correlated with the occurrence of axonal arbors observed in layers 2 and 3 of different species of monkeys: bush babies (Diamond et al., 1985; Lachica and Casagrande, 1992), owl monkeys (Ding and Casagrande, 1997), squirrel monkeys (Fitzpatrick et al., 1983), and macaques (Casagrande et al., 2007). We found that the highest density of VGluT2-ir puncta in layers 2 and 3 corresponds to the CO-rich patches in layers 2 and 3, suggesting colocalization with the thalamic afferent terminations reported after anterograde tracer injections into the LGN (Fitzpatrick et al., 1983; Horton, 1984; Diamond et al., 1985; Lachica and Casagrande, 1992; Ding and Casagrande, 1997; Casagrande et al., 2007).

Layer 1 of V1 cortex receives LGN afferents (Hubel and Wiesel, 1972; Lund, 1973; Benevento and Rezak, 1975; Ogren and Hendrickson, 1977; Hendrickson et al., 1978; Rezak and Benevento, 1979). Studies using injections of HRP into the LGN confirmed the presence of fine thalamic afferents from the LGN into layer 1 (Blasdel and Lund, 1983) and they were particularly focused in the outer portion of layer 1 (Fitzpatrick et al., 1983; Diamond et al., 1985). More recently, it was established that K neurons from the LGN are responsible for these collateral branches that project broadly in layer 1 (Ding and Casagrande, 1997; Casagrande et al., 2007), with LGN layer K1 and K2 subtypes being mainly responsible for projections in layer 1 in macaque V1 (Casagrande et al., 2007). Our results demonstrate the presence of VGluT2-ir puncta in layer 1, suggesting that VGluT2 IHC is sensitive enough to show the thalamic afferents in this layer. We also observed that some fibers reaching layer 1 appeared to come from collaterals from the VGluT2-ir fibers in layers 2 and 3. Interestingly, Casagrande and colleagues (2007) observed direct projections to layer 1 from K neurons (layer K1–K2), or from collaterals of the projections to the CO-rich patches (layer K3–K6). Therefore, it is likely that the VGluT2-ir puncta we observed in layers 1 and 2/3 came from all the subdivisions of the K-layer input to the striate cortex from the LGN in addition to the projections from the pulvinar. This means that VGluT2 is sensitive enough to show this projection as well as the projections from the M- and P-layers of the LGN.

Layer 6 is also a recipient of LGN thalamic afferents (Hubel and Wiesel, 1972; Lund and Boothe, 1975; Hendrickson et al., 1978). We found a clear distribution of VGluT2-ir puncta in layer 6, with the highest density in the mid-upper region of layer 6, forming an annular pattern clearly visible in horizontal sections (Fig. 6H). Previous anterograde studies found that the projections from parvocellular neurons of LGN targeted mainly layers 4Cβ and 4A, but also sent axon collaterals to the upper half of layer 6 (Hendrickson et al., 1978). The VGluT2-ir puncta in the upper half of layer 6 could be the same as the axonal arborization shown by Hendrickson et al. (1978). Interestingly, Figure 6 of Hendrickson et al. (1978) shows a patchy pattern in the upper half of layer 6 in parasagittal sections. VGluT2 patches in layer 6 were more closely spaced (30–100 μm; Fig. 6H) than the VGluT2 and matched CO patches in layers 2 and 3. If this patchy pattern is a result of collateral axonal projections from parvocellular neurons, it may correspond to the patchy distribution reported by Hendrickson et al. (1978). The lower half of layer 6 showed a low density of VGluT2-ir puncta in our macaque tissue, which presumably arises from the magnocellular layers of the LGN (Hendrickson et al., 1978; Blasdel and Lund, 1983). Previous studies showed that these collaterals were extremely fine and unlikely to be seen except with the dense filling achieved by intracellular injection (Blasdel and Lund, 1983).

Although the overall pattern of VGluT2-ir puncta density correlates very closely with the known distribution of afferent terminals from the LGN to V1, it is likely that some of the VGluT2-ir puncta found in V1 are associated with afferents from other thalamic or subthalamic structures. There are numerous reports of a direct projection to layers 1 and 2/3 of V1 from the pulvinar, mainly from the inferior pulvinar and the lateral pulvinar (Ogren and Hendrickson, 1977; Rezak and Benevento, 1979; Kennedy and Bullier, 1985; Perkel et al., 1986; Adams et al., 2000; Rockland et al., 1999; Kaas and Lyon, 2007; Baldwin et al., 2011), and at the border between layers 1 and 2 from the amygdala (Freese and Amaral, 2005, 2006). A comparison of retrogradely labeled neurons in the different subdivisions of the pulvinar, after injections of retrograde tracer in V1 and V2, showed a higher percentage of labeled neurons in V2 than in V1 (78 and 22%, respectively) (Kennedy and Bullier, 1985). In addition, Kennedy and Bullier (1985) observed a small number of

labeled neurons in other subcortical structures, including the intralaminar nuclei, the nucleus basalis of Meynert, the amygdala, and the claustrum after injections of retrograde tracer in V1. However, the quantification of the strength of these afferents to V1 or V2 could not be established because of the small number of labeled neurons. Thus, the pattern of VGluT2-ir puncta found in V1 is most likely to be mainly due to thalamic afferents arising from the LGN, with a small contribution from other subcortical neurons projecting to V1.

Comparison with other marking methods

Classical techniques for identifying terminal distributions such as degeneration of axons after lesions (e.g., Jones and Powell, 1970; Peters and Feldman, 1976; Davis and Sterling, 1979), recent tracing techniques such as intracellular filling of individual axons in the optic radiation (e.g., Blasdel and Lund, 1983; Friedlander and Martin, 1989; Anderson et al., 1992), or anterograde tract-tracer injection into the LGN (e.g., McGuire et al., 1984; LeVay, 1986; Kharazia and Weinberg, 1993; Ahmed et al., 1994; Herrmann et al., 1994) all require manipulations (lesions or injections) prior to processing for terminal distributions, and often depend critically on timing and sensitivity. Other techniques for specific afferent labeling (DeFelipe and Jones, 1991; Latawiec et al., 2000) take advantage of parvalbumin as a marker for thalamic relay cells and their axon terminals in monkey V1 (Jones and Hendry, 1989). However, this approach requires analysis at the EM level, as it is necessary to distinguish the PV-ir thalamo-cortical terminals from the PV-ir cortico-cortical afferents because the thalamo-cortical afferents are glutamatergic asymmetrical synapses, whereas the cortico-cortical terminals are GABAergic symmetric synapses. If VGluT2 is shown to localize with specific afferent terminals, as we have hypothesized for monkey, and as has been shown in ferret (Nahmani and Erisir, 2005) and mouse (Coleman et al., 2010), then it is a valuable tool for quantifying the density of the complete terminal distribution in the cortex.

VGluT2-ir puncta in human V1

The current study relies on the correlation between the VGluT2-ir pattern in non-human primate and the known LGN thalamic afferent terminal distribution, to infer that VGluT2 labels the LGN afferent terminals in human V1. As far as we know, only one study has shown the thalamic afferent terminations in the visual cortex of humans; this was after degeneration of the LGN fibers after a thalamic lesion (Miklossy, 1992). As in macaque, VGluT2 IHC in human shows a specific laminar pattern.

The principal LGN thalamic recipient layer, 4C, showed the highest level of VGluT2-ir supporting the result of the degeneration observed after thalamic lesions (Miklossy, 1992). Within layer 4C, the density of VGluT2-ir puncta decreases from layer 4Cβ to 4Cα. Our data on the size of the minicolumns (24.7 μm for layer 4Cβ) agree with previous studies in human V1 that found a minicolumnar width of 24 μm in layer 3 (Buxhoeveden et al., 1996) but not with estimates for layer 4 (18.6 μm) (Casanova et al., 2009), which is considerably narrower than that found in the current study. However, the core width of 10.5 μm (Casanova et al., 2009) is similar to our estimate of 11.9 μm. Our data also show an increase in the minicolumn width from macaque to human (from 18.0 to 24.7 μm, respectively). The ratio of core width to the minicolumn width remains constant in the macaque and human (0.49) due to the increase of the core width from 8.9 μm in macaque, to 11.9 μm in human. The ratio we find (0.49) is smaller by about 10% than the ratio (0.57) previously reported for human and macaque (Casanova et al., 2009).

The current study established that most of layer 4B in human cortex is devoid of VGluT2-ir puncta, but nonetheless not completely lacking, as we found a few regions with a low density of VGluT2-ir puncta (Fig. 4). Previously it had been suggested that there might be graded direct afferent input to layer 4B (Preuss et al., 1999). Functionally, this result means that layer 4B in human appears anatomically similar to 4B in macaque, although we did find that it occupied relatively less of the layer 4 extent in human than in macaque.

Layer 4A of human has patches of VGluT2-ir puncta arranged horizontally, but they do not form the characteristic honeycomb pattern observed in macaque, which is seen as regions of high and low density with layer 4A parasagittal and coronal sections. In addition, the density of VGluT2 is considerably lower in human than in macaque. Previous studies using CO histochemistry also failed to find any structural organization resembling the honeycomb arrangement found in macaque layer 4A (Horton, 1984; Wong-Riley et al., 1993). However, a lightly immunostained calbindin-ir band of neurons was observed in layer 4A (Hendry and Carder, 1993; Yoshioka and Hendry, 1995), and also observed in tissue processed for non-phosphorylated neurofilaments (NFNP, anti-SMI-32 (Yoshioka and Hendry, 1995); Preuss et al., 1999), MAP and anti-MAP2 (Preuss et al., 1999), and Cat-301 (Preuss and Coleman, 2002).

In general, these markers mainly occupied the upper part of layer 4B (Hendrickson et al., 1978), with clusters of immunostained neurons and processes extending into layer 4A. Although some investigators have tentatively associated the structural organization in human layer 4A with the honeycomb organization found in macaque layer 4A (Yoshioka and Hendry, 1995), there are major

differences between the two species. It appears that the mesh-like pattern found in macaque is specifically related to the pattern of LGN thalamic terminals (Casagrande et al., 2007), whereas there is no such arrangement in human 4A. Macaque layer 4A is a recipient of the P-pathway (Hubel and Wiesel, 1972; Hendrickson et al., 1978), however, in humans, the presence of P-pathway afferents is more controversial. One proposal is that it has completely disappeared or is clearly reduced in humans compared with macaques (Preuss et al., 1999; Preuss and Coleman, 2002).

Our data show that there are relatively few VGlutT-ir puncta above layer 4Cα in 4B, ruling out the likelihood that there is a substantial direct input from the M-pathway to dendrites in layer 4B. In contrast, we did observe sparse afferent terminations in layer 4A, but whether these afferents are from the M-, P-, or K-pathways cannot be determined. An alternative explanation is that a subset of LGN afferents projecting to layer 4A in human does not express VGluT2. If this was the case, then there may be functional input from LGN to layer 4A that is not matched to either VGluT2 or CO staining. We think this alternative explanation is unlikely. How the P- and K-pathways evolved in different primate species is an intriguing question.

Above layer 4A, there are patches of VGluT2-ir puncta in layer 3 that in some cases project into layer 2. The interpatch distance of about 800 μm is similar to the range of spacing 600–800 μm or 500–800 μm between CO-rich patches in human layers 2 and 3 found by Horton and Hedley-Whyte (1984) and Wong-Riley et al. (1993), respectively. However, in some regions we could not find clearly defined patches. We do not know if the lack of regular patches is due to the condition of the tissue, or to a genuine difference between human and macaque supragranular organization.

Layer 6 in human does have a substantial density of VGluT2-ir puncta, running in a continuous band of about 150 μm wide in the mid-region of the layer. Other studies have observed a light band of CO in layer 6 (Horton and Hedley-Whyte, 1984; Wong-Riley et al., 1993), as well as a geniculocortical fiber degeneration of fine terminal branches mostly found in the lower half of layer 6 (Miklossy, 1992). Our impression is that there is a higher density of puncta in human than in macaque layer 6, but verification will need to be made with quantitative puncta counts. Although there was a continuous distribution of puncta in mid-layer 6, the density appeared periodic, as found in macaque. In contrast, CO did not show these variations in density. Finally, VGluT2-ir puncta are also observed in layer 1, suggesting it is a recipient of thalamic afferents as observed in macaque (Fitzpatrick et al., 1983; Diamond et al., 1985; Lachica and Casagrande, 1992; Ding and Casagrande, 1997; Casagrande et al., 2007).

Presence of VGluT2-ir puncta in V2

In addition to the presence of VGluT2-ir puncta in V1, we also observed a preferential distribution of VGluT2-ir puncta in layers 1, 3, and 4 of V2, which qualitatively matches the distribution of the anterogradely labeled terminals in V2 after injections into the lateral pulvinar. There were also differences: anterograde labeling shows patchy input to lower layer 3 and upper layer 4, and very light input extending up to layer 1 (Benevento and Rezak, 1975; Trojanowski and Jacobson, 1976; Levitt et al., 1995; Rockland et al., 1999), whereas VGluT2 is continuous in lower layer 3/upper layer 4 with a high density of puncta in layer 1, especially in macaque. Scattered and lower density of boutons was also described in layers 5 and 6 after injections in the lateral pulvinar (Levitt et al., 1995; Rockland et al., 1999). There was a low density of VGluT2-ir puncta in layers 5 and 6 (Fig. 8J–L [macaque] and P,Q [human]). There was also a low density of puncta in layer 2 (Fig. 8F,G [macaque] and M [human]). Other subthalamic nuclei could also contribute to the presence of VGluT2-ir puncta into V2 (Bullier and Kennedy, 1983). Colocalization studies after injection of tracer into specific thalamic and subthalamic nuclei with VGluT2 are required to unequivocally identify the origin of all VGluT2-ir terminals in V2.

Qualitatively, the sizes of VGluT2-ir puncta in 4C are larger than VGluT1-ir terminals (Fig. 1) and this corresponds to the known difference in size between the thalamo-cortical and intracortical terminals (Nahnami and Erisir, 2005). It has also been shown recently that the pulvinar terminals in V2 are smaller than those from the LGN to layer 4C of V1 (Marion et al., 2011). In the region of the V1/V2 border, we found that the VGluT2-ir puncta were of different sizes. The smallest are prominent in V2, and the largest, which could be axonal collaterals from LGN axons, branch in V1 and V2. Based on these findings, we suggest that this size difference could correspond with a functional difference in the input to these areas (Sherman and Guillery, 1998). EM studies would be necessary to confirm this point.

Functional implications

One of the main differences between the LGN thalamic afferents to visual cortex between human and macaques is the lack of the honeycomb pattern characteristic of the macaque layer 4A (Horton and Hedley-Whyte, 1984; Wong-Riley et al., 1993). Due to this lack of CO-dense staining in layer 4A, Preuss and colleagues (Preuss et al., 1999; Preuss and Coleman, 2002) have speculated that there is a reduction or lack of LGN thalamic afferent

inputs to layer 4A in human, specifically a reduction of the parvocellular geniculate projection to this layer. In macaque, it is well established that the P-pathway provides the main afferent input to 4A (Fitzpatrick et al., 1985; Peters and Sethares, 1991a; Hendry and Yoshioka, 1994), although there is also an additional input from the K-pathway (layers K3–K6) (Casagrande et al., 2007).

Additionally, in macaque it has been shown that there is blue-off afferent input to layer 4A (Chatterjee and Callaway, 2003); the blue-off neurons in the retina include midget ganglion cells (Klug et al., 2003; Field et al., 2010) that belong to the P-pathway in macaque, providing a further link between the P-pathway input to layer 4A. Interestingly, the size of the K axons is much finer than those of P and M cells (Casagrande et al., 2007), and therefore it may be the case that the remaining K-fiber inputs are not revealed by CO histochemistry, but are better revealed with the more sensitive and precise VGluT2 IHC technique presented in this study. If one of the functions of the LGN input to 4A in macaque is to provide chromatic input from the S-cone pathway (Chatterjee and Callaway, 2003), then this may not be the case in humans. There are no substantial low-level perceptual differences between macaques and humans in blue/yellow color vision, which is generally associated with the S-cone pathway, and therefore it might be that this aspect of color processing is not closely associated with layer 4A in humans.

ACKNOWLEDGMENT

We thank A. Erisir for her kind advice about the protocol, J. DeFelipe for funding from the Spanish Ministry of Education, Science, and Innovation, and J. Levitt for critical reading of the manuscript.

CONFLICT OF INTEREST STATEMENT

The authors declare that no conflict of interest is related to this work.

ROLE OF AUTHORS

All authors had full access to all the data in the study and take responsibility for the integrity of the data and the accuracy of the data analysis. Study concept and design: V.G.-M. and M.J.H. Acquisition of data: V.G.-M., T.H.A., and Y.C.A. Analysis and interpretation of data: V.G.-M. and M.J.H. Drafting of the manuscript: V.G.-M. and M.J.H. Critical revision of the manuscript for important intellectual content: V.G.-M. and M.J.H. Obtained funding: V.G.-M. and M.J.H. Technical and material support: T.H.A. and Y.C.A. Study supervision: M.J.H.

LITERATURE CITED

Adams MM, Hof PR, Gattass R, Webster MJ, Ungerleider LG. 2000. Visual cortical projections and chemoarchitecture of macaque monkey pulvinar. J Comp Neurol 419: 377–393.

Ahmed B, Anderson JC, Douglas RJ, Martin KA, Nelson JC. 1994. Polyneuronal innervation of spiny stellate neurons in cat visual cortex. J Comp Neurol 341:39–49.

Alonso-Nanclares L. 2005. Vesicular glutamate transporter 1 immunostaining in the normal and epileptic human cerebral cortex. Neuroscience 134:59–68.

Alonso-Nanclares L, Minelli A, Melone M, Edwards RH, Defelipe J, Conti F. 2004. Perisomatic glutamatergic axon terminals: a novel feature of cortical synaptology brevealed by vesicular glutamate transporter 1 immunostaining. Neuroscience 123:547–556.

Anderson JC, Martin KA, Picanco-Diniz CW. 1992. The neurons in layer 1 of cat visual cortex. Proc R Soc Lond B 248: 27–33.

Balaram P, Kaas JH. 2011. VGLUT1 and VGLUT2 expression in the visual system of Old World, New World and prosimian primates. Washington, DC: Society for Neuroscience, 2011. Online.

Baldwin MK, Kaskan PM, Zhang B, Chino YM, Kaas JH. 2012. Cortical and subcortical connections of V1 and V2 in early postnatal macaque monkeys. J Comp Neurol 520:544–569.

Bankfalvi A, Navabi H, Bier B, Bocker W, Jasani B, Schmid KW. 1994. Wet autoclave pretreatment for antigen retrieval in diagnostic immunohistochemistry. J Pathol 174: 223–228.

Benevento LA, Rezak M. 1975. Extrageniculate projections to layers VI and I of striate cortex (area 17) in the rhesus monkey (*Macaca mulatta*). Brain Res 96:51–55.

Blasdel GG, Lund JS. 1983. Termination of afferent axons in macaque striate cortex. J Neurosci 3:1389–1413.

Blazquez-Llorca L, Garcia-Marin V, DeFelipe J. 2010. GABAergic complex basket formations in the human neocortex. J Comp Neurol 518:4917–4937.

Boulland JL, Qureshi T, Seal RP, Rafiki A, Gundersen V, Bergersen LH, Fremeau RT Jr, Edwards RH, Storm-Mathisen J, Chaudhry FA. 2004. Expression of the vesicular glutamate transporters during development indicates the widespread corelease of multiple neurotransmitters. J Comp Neurol 480:264–280.

Boulland JL, Ferhat L, Tallak Solbu T, Ferrand N, Chaudhry FA, Storm-Mathisen J, Esclapez M. 2007. Changes in vesicular transporters for gamma-aminobutyric acid and glutamate reveal vulnerability and reorganization of hippocampal neurons following pilocarpine-induced seizures. J Comp Neurol 503:466–485.

Brodmann K. 1909. Localisation in the cerebral cortex. Garey LJ, translator. London: Smith-Gordon.

Buxhoeveden D, Lefkowitz W, Loats P, Armstrong E. 1996. The linear organization of cell columns in human and nonhuman anthropoid Tpt cortex. Anat Embryol (Berl) 194:23–36.

Callaway EM. 1998. Local circuits in primary visual cortex of the macaque monkey. Annu Rev Neurosci 21:47–74.

Carroll EW, Wong-Riley MT. 1984. Quantitative light and electron microscopic analysis of cytochrome oxidase-rich zones in the striate cortex of the squirrel monkey. J Comp Neurol 222:1–17.

Casagrande VA. 1994. A third parallel visual pathway to primate area V1. Trends Neurosci 17:305–310.

Casagrande VA, Norton TT. 1991. Lateral geniculate nucleus: a review of its physiology and function. In: Leventhal AG, editor. The neural basis of visual function: vision and visual dysfunction. London: McMillan Press, p 41–84.

Casagrande VA, Yazar F, Jones KD, Ding Y. 2007. The morphology of the koniocellular axon pathway in the macaque monkey. Cereb Cortex 17:2334–2345.

Casanova MF, Trippe J 2nd, Tillquist C, Switala AE. 2009. Morphometric variability of minicolumns in the striate cortex of *Homo sapiens*, *Macaca mulatta*, and *Pan troglodytes*. J Anat 214:226–234.

Celio MR, Scharer L, Morrison JH, Norman AW, Bloom FE. 1986. Calbindin immunoreactivity alternates with cytochrome c-oxidase-rich zones in some layers of the primate visual cortex. Nature 323:715–717.

Celio MR, Baier W, Scharer L, Gregersen HJ, de Viragh PA, Norman AW. 1990. Monoclonal antibodies directed against the calcium binding protein Calbindin D-28k. Cell Calcium 11:599–602.

Chatterjee S, Callaway EM. 2003. Parallel colour-opponent pathways to primary visual cortex. Nature 426:668–671.

Coleman JE, Nahmani M, Gavornik JP, Haslinger R, Heynen AJ, Erisir A, Bear MF. 2010. Rapid structural remodeling of thalamocortical synapses parallels experience-dependent functional plasticity in mouse primary visual cortex. J Neurosci 30:9670–9682.

Conley M, Fitzpatrick D. 1989. Morphology of retinogeniculate axons in the macaque. Vis Neurosci 2:287–296.

Davis TL, Sterling P. 1979. Microcircuitry of cat visual cortex: classification of neurons in layer IV of area 17, and identification of the patterns of lateral geniculate input. J Comp Neurol 188:599–627.

DeFelipe J. 1997. Types of neurons, synaptic connections and chemical characteristics of cells immunoreactive for calbindin-D28K, parvalbumin and calretinin in the neocortex. J Chem Neuroanat 14:1–19.

DeFelipe J. 2002. Cortical interneurons: from Cajal to 2001. Prog Brain Res 136:215–238.

DeFelipe J, Jones EG. 1991. Parvalbumin immunoreactivity reveals layer IV of monkey cerebral cortex as a mosaic of microzones of thalamic afferent terminations. Brain Res 562:39–47.

DeFelipe J, Ballesteros-Yanez I, Inda MC, Munoz A. 2006. Double-bouquet cells in the monkey and human cerebral cortex with special reference to areas 17 and 18. Prog Brain Res 154:15–32.

Diamond IT, Conley M, Itoh K, Fitzpatrick D. 1985. Laminar organization of geniculocortical projections in *Galago senegalensis* and *Aotus trivirgatus*. J Comp Neurol 242:584–610.

Ding Y, Casagrande VA. 1997. The distribution and morphology of LGN K pathway axons within the layers and CO blobs of owl monkey V1. Vis Neurosci 14:691–704.

Douglas RJ, Martin KA. 1991. A functional microcircuit for cat visual cortex. J Physiol 440:735–769.

Field GD, Gauthier JL, Sher A, Greschner M, Machado TA, Jepson LH, Shlens J, Gunning DE, Mathieson K, Dabrowski W, Paninski L, Litke AM, Chichilnisky EJ. 2010. Functional connectivity in the retina at the resolution of photoreceptors. Nature 467:673–677.

Fitzpatrick D, Itoh K, Diamond IT. 1983. The laminar organization of the lateral geniculate body and the striate cortex in the squirrel monkey (*Saimiri sciureus*). J Neurosci 3: 673–702.

Fitzpatrick D, Lund JS, Blasdel GG. 1985. Intrinsic connections of macaque striate cortex: afferent and efferent connections of lamina 4C. J Neurosci 5:3329–3349.

Freese JL, Amaral DG. 2005. The organization of projections from the amygdala to visual cortical areas TE and V1 in the macaque monkey. J Comp Neurol 486:295–317.

Freese JL, Amaral DG. 2006. Synaptic organization of projections from the amygdala to visual cortical areas TE and V1 in the macaque monkey. J Comp Neurol 496:655–667.

Fremeau RT Jr, Troyer MD, Pahner I, Nygaard GO, Tran CH, Reimer RJ, Bellocchio EE, Fortin D, Storm-Mathisen J, Edwards RH. 2001. The expression of vesicular glutamate transporters defines two classes of excitatory synapse. Neuron 31:247–260.

Fremeau RT Jr, Burman J, Qureshi T, Tran CH, Proctor J, Johnson J, Zhang H, Sulzer D, Copenhagen DR, Storm-Mathisen J, Reimer RJ, Chaudhry FA, Edwards RH. 2002. The identification of vesicular glutamate transporter 3 suggests novel modes of signaling by glutamate. Proc Natl Acad Sci U S A 99:14488–14493.

Fremeau RT Jr, Voglmaier S, Seal RP, Edwards RH. 2004. VGLUTs define subsets of excitatory neurons and suggest novel roles for glutamate. Trends Neurosci 27:98–103.

Freund TF, Martin KA, Soltesz I, Somogyi P, Whitteridge D. 1989. Arborisation pattern and postsynaptic targets of physiologically identified thalamocortical afferents in striate cortex of the macaque monkey. J Comp Neurol 289: 315–336.

Friedlander MJ, Martin KA. 1989. Development of Y-axon innervation of cortical area 18 in the cat. J Physiol 416: 183–213.

Fujiyama F, Furuta T, Kaneko T. 2001. Immunocytochemical localization of candidates for vesicular glutamate transporters in the rat cerebral cortex. J Comp Neurol 435:379–387.

Fujiyama F, Hioki H, Tomioka R, Taki K, Tamamaki N, Nomura S, Okamoto K, Kaneko T. 2003. Changes of immunocytochemical localization of vesicular glutamate transporters in the rat visual system after the retinofugal denervation. J Comp Neurol 465:234–249.

Fyk-Kolodziej B, Dzhagaryan A, Qin P, Pourcho RG. 2004. Immunocytochemical localization of three vesicular glutamate transporters in the cat retina. J Comp Neurol 475: 518–530.

Garcia-Cabezas MA, Rico B, Sanchez-Gonzalez MA, Cavada C. 2007. Distribution of the dopamine innervation in the macaque and human thalamus. Neuroimage 34:965–984.

Garcia-Marin V, Blazquez-Llorca L, Rodriguez JR, Gonzalez-Soriano J, DeFelipe J. 2010. Differential distribution of neurons in the gyral white matter of the human cerebral cortex. J Comp Neurol 518:4740–4759.

Garey LJ, Powell TP. 1971. An experimental study of the termination of the lateral geniculo-cortical pathway in the cat and monkey. Proc R Soc Lond B 179:41–63.

Gras C, Herzog E, Bellenchi GC, Bernard V, Ravassard P, Pohl M, Gasnier B, Giros B, El Mestikawy S. 2002. A third vesicular glutamate transporter expressed by cholinergic and serotoninergic neurons. J Neurosci 22:5442–5451.

Graziano A, Liu XB, Murray KD, Jones EG. 2008. Vesicular glutamate transporters define two sets of glutamatergic afferents to the somatosensory thalamus and two thalamocortical projections in the mouse. J Comp Neurol 507:1258–1276.

Hackett TA, de la Mothe LA. 2009. Regional and laminar distribution of the vesicular glutamate transporter, VGluT2, in the macaque monkey auditory cortex. J Chem Neuroanat 38:106–116.

Hawken MJ, Parker AJ, Lund JS. 1988. Laminar organization and contrast sensitivity of direction-selective cells in the striate cortex of the Old World monkey. J Neurosci 8:3541–3548.

Hendrickson AE, Wilson JR, Ogren MP. 1978. The neuroanatomical organization of pathways between the dorsal lateral geniculate nucleus and visual cortex in Old World and New World primates. J Comp Neurol 182:123–136.

Hendry SH, Carder RK. 1993. Neurochemical compartmentation of monkey and human visual cortex: similarities and variations in calbindin immunoreactivity across species. Vis Neurosci 10:1109–1120.

Hendry SH, Yoshioka T. 1994. A neurochemically distinct third channel in the macaque dorsal lateral geniculate nucleus. Science 264:575–577.

Herrmann K, Antonini A, Shatz CJ. 1994. Ultrastructural evidence for synaptic interactions between thalamocortical axons and subplate neurons. Eur J Neurosci 6:1729–1742.

Herzog E, Bellenchi GC, Gras C, Bernard V, Ravassard P, Bedet C, Gasnier B, Giros B, El Mestikawy S. 2001. The existence

of a second vesicular glutamate transporter specifies subpopulations of glutamatergic neurons. J Neurosci 21:RC181.
Herzog E, Takamori S, Jahn R, Brose N, Wojcik SM. 2006. Synaptic and vesicular co-localization of the glutamate transporters VGLUT1 and VGLUT2 in the mouse hippocampus. J Neurochem 99:1011–1018.
Horton JC. 1984. Cytochrome oxidase patches: a new cytoarchitectonic feature of monkey visual cortex. Phil Trans R Soc Lond B 304:199–253.
Horton JC, Hedley-Whyte ET. 1984. Mapping of cytochrome oxidase patches and ocular dominance columns in human visual cortex. Phil Trans R Soc Lond B 304:255–272.
Horton JC, Hubel DH. 1981. Regular patchy distribution of cytochrome oxidase staining in primary visual cortex of macaque monkey. Nature 292:762–764.
Horton JC, Dagi LR, McCrane EP, de Monasterio FM. 1990. Arrangement of ocular dominance columns in human visual cortex. Arch Ophthalmol 108:1025–1031.
Hubel DH, Wiesel TN. 1969. Anatomical demonstration of columns in the monkey striate cortex. Nature 221:747–750.
Hubel DH, Wiesel TN. 1972. Laminar and columnar distribution of geniculo-cortical fibers in the macaque monkey. J Comp Neurol 146:421–450.
Hubel DH, Wiesel TN, LeVay S. 1977. Plasticity of ocular dominance columns in monkey striate cortex. Phil Trans R Soc Lond B 278:377–409.
Inda MC, Defelipe J, Munoz A. 2007. The distribution of chandelier cell axon terminals that express the GABA plasma membrane transporter GAT-1 in the human neocortex. Cereb Cortex 17:2060–2071.
Jiao Y, Sun Z, Lee T, Fusco FR, Kimble TD, Meade CA, Cuthbertson S, Reiner A. 1999. A simple and sensitive antigen retrieval method for free-floating and slide-mounted tissue sections. J Neurosci Methods 93:149–162.
Jones EG, Burton H. 1974. Cytoarchitecture and somatic sensory connectivity of thalamic nuclei other than the ventrobasal complex in the cat. J Comp Neurol 154:395–432.
Jones EG, Hendry SH. 1989. Differential calcium binding protein immunoreactivity distinguishes classes of relay neurons in monkey thalamic nuclei. Eur J Neurosci 1:222–246.
Jones EG, Powell TP. 1970. An anatomical study of converging sensory pathways within the cerebral cortex of the monkey. Brain 93:793–820.
Kaas JH, Huerta MF. 1988. Subcortical visual system of primates. In: Steklis HP, editor. Comparative primate biology. New York: Alan R. Liss, p 327–391.
Kaas JH, Lyon DC. 2007. Pulvinar contributions to the dorsal and ventral streams of visual processing in primates. Brain Res Rev 55:285–296.
Kameda H, Hioki H, Tanaka YH, Tanaka T, Sohn J, Sonomura T, Furuta T, Fujiyama F, Kaneko T. 2012. Parvalbumin-producing cortical interneurons receive inhibitory inputs on proximal portions and cortical excitatory inputs on distal dendrites. Eur J Neurosci 35:838–854.
Kennedy H, Bullier J. 1985. A double-labeling investigation of the afferent connectivity to cortical areas V1 and V2 of the macaque monkey. J Neurosci 5:2815–2830.
Kharazia VN, Weinberg RJ. 1993. Glutamate in terminals of thalamocortical fibers in rat somatic sensory cortex. Neurosci Lett 157:162–166.
Klug K, Herr S, Ngo IT, Sterling P, Schein S. 2003. Macaque retina contains an S-cone OFF midget pathway. J Neurosci 23:9881–9887.
Lachica EA, Casagrande VA. 1992. Direct W-like geniculate projections to the cytochrome oxidase (CO) blobs in primate visual cortex: axon morphology. J Comp Neurol 319:141–158.
Latawiec D, Martin KA, Meskenaite V. 2000. Termination of the geniculocortical projection in the striate cortex of macaque monkey: a quantitative immunoelectron microscopic study. J Comp Neurol 419:306–319.
LeVay S. 1986. Synaptic organization of claustral and geniculate afferents to the visual cortex of the cat. J Neurosci 6: 3564–3575.
Leventhal AG, Rodieck RW, Dreher B. 1981. Retinal ganglion cell classes in the Old World monkey: morphology and central projections. Science 213:1139–1142.
Levitt JB, Yoshioka T, Lund JS. 1995. Connections between the pulvinar complex and cytochrome oxidase-defined compartments in visual area V2 of macaque monkey. Exp Brain Res 104:419–430.
Livingstone MS, Hubel DH. 1982. Thalamic inputs to cytochrome oxidase-rich regions in monkey visual cortex. Proc Natl Acad Sci U S A 79:6098–6101.
Livingstone MS, Hubel DH. 1988. Do the relative mapping densities of the magno- and parvocellular systems vary with eccentricity? J Neurosci 8:4334–4339.
Lund JS. 1973. Organization of neurons in the visual cortex, area 17, of the monkey (*Macaca mulatta*). J Comp Neurol 147:455–496.
Lund JS. 1988. Anatomical organization of macaque monkey striate visual cortex. Annu Rev Neurosci 11:253–288.
Lund JS, Boothe RG. 1975. Interlaminar connections and pyramidal neuron organisation in the visual cortex, area 17, of the macaque monkey. J Comp Neurol 159:305–334.
Marion RT, LI K, Purushothaman G, Yampolsky D, Jiang Y, Julia M-H, Casagrande V. 2011. A quantitative comparison between geniculate axons in V1 and pulvinar axons in V2 Washington, DC: Society for Neuroscience, 2011. Online.
Mates SL, Lund JS. 1983. Neuronal composition and development in lamina 4C of monkey striate cortex. J Comp Neurol 221:60–90.
McGuire BA, Hornung JP, Gilbert CD, Wiesel TN. 1984. Patterns of synaptic input to layer 4 of cat striate cortex. J Neurosci 4:3021–3033.
McLaughlin D, Shapley R, Shelley M, Wielaard DJ. 2000. A neuronal network model of macaque primary visual cortex (V1): orientation selectivity and dynamics in the input layer 4Calpha. Proc Natl Acad Sci U S A 97:8087–8092.
Merchan-Perez A, Rodriguez JR, Ribak CE, DeFelipe J. 2009. Proximity of excitatory and inhibitory axon terminals adjacent to pyramidal cell bodies provides a putative basis for nonsynaptic interactions. Proc Natl Acad Sci U S A 106:9878–9883.
Miklossy J. 1992. The geniculocalcarine pathway in man, and some putative rostral visual areas involved in visuo-spatial attention. In: Gulyas B, Ottoson D, Roland PE, editors. Functional organisation of the human visual cortex. Oxford, UK: Pergamon Press. p 123–136.
Mountcastle VB. 1997. The columnar organization of the neocortex. Brain 120:701–722.
Nahmani M, Erisir A. 2005. VGluT2 immunochemistry identifies thalamocortical terminals in layer 4 of adult and developing visual cortex. J Comp Neurol 484:458–473.
Nakamura K, Hioki H, Fujiyama F, Kaneko T. 2005. Postnatal changes of vesicular glutamate transporter (VGluT)1 and VGluT2 immunoreactivities and their colocalization in the mouse forebrain. J Comp Neurol 492:263–288.
Nakamura K, Watakabe A, Hioki H, Fujiyama F, Tanaka Y, Yamamori T, Kaneko T. 2007. Transiently increased colocalization of vesicular glutamate transporters 1 and 2 at single axon terminals during postnatal development of mouse neocortex: a quantitative analysis with correlation coefficient. Eur J Neurosci 26:3054–3067.
Ogren MP, Hendrickson AE. 1977. The distribution of pulvinar terminals in visual areas 17 and 18 of the monkey. Brain Res 137:343–350.
Ong WY, Garey LJ. 1990. Neuronal architecture of the human temporal cortex. Anat Embryol (Berl) 181:351–364.

Perkel DJ, Bullier J, Kennedy H. 1986. Topography of the afferent connectivity of area 17 in the macaque monkey: a double-labelling study. J Comp Neurol 253:374–402.

Peters A, Payne BR. 1993. Numerical relationships between geniculocortical afferents and pyramidal cell modules in cat primary visual cortex. Cereb Cortex 3:69–78.

Peters A. 1994. The organization of the primary visual cortex in the macaque. In: Peters A, Jones EG, editors. Cerebral cortex: primary visual cortex in primates. New York: Plenum Press

Peters A, Feldman ML. 1976. The projection of the lateral geniculate nucleus to area 17 of the rat cerebral cortex. I. General description. J Neurocytol 5:63–84.

Peters A, Sethares C. 1991a. Layer IVA of rhesus monkey primary visual cortex. Cereb Cortex 1:445–462.

Peters A, Sethares C. 1991b. Organization of pyramidal neurons in area 17 of monkey visual cortex. J Comp Neurol 306:1–23.

Pileri SA, Roncador G, Ceccarelli C, Piccioli M, Briskomatis A, Sabattini E, Ascani S, Santini D, Piccaluga PP, Leone O, Damiani S, Ercolessi C, Sandri F, Pieri F, Leoncini L, Falini B. 1997. Antigen retrieval techniques in immunohistochemistry: comparison of different methods. J Pathol 183: 116–123.

Preuss TM, Coleman GQ. 2002. Human-specific organization of primary visual cortex: alternating compartments of dense Cat-301 and calbindin immunoreactivity in layer 4A. Cereb Cortex 12:671–691.

Preuss TM, Qi H, Kaas JH. 1999. Distinctive compartmental organization of human primary visual cortex. Proc Natl Acad Sci U S A 96:11601–11606.

Rezak M, Benevento LA. 1979. A comparison of the organization of the projections of the dorsal lateral geniculate nucleus, the inferior pulvinar and adjacent lateral pulvinar to primary visual cortex (area 17) in the macaque monkey. Brain Res 167:19–40.

Rockland KS, Andresen J, Cowie RJ, Robinson DL. 1999. Single axon analysis of pulvinocortical connections to several visual areas in the macaque. J Comp Neurol 406:221–250.

Schafer MK, Varoqui H, Defamie N, Weihe E, Erickson JD. 2002. Molecular cloning and functional identification of mouse vesicular glutamate transporter 3 and its expression in subsets of novel excitatory neurons. J Biol Chem 277:50734–50748.

Seldon HL. 1981. Structure of human auditory cortex. I. Cytoarchitectonics and dendritic distributions. Brain Res 229:277–294.

Seldon HL. 1982. Structure of human auditory cortex. III. Statistical analysis of dendritic trees. Brain Res 249:211–221.

Sherman SM, Guillery RW. 1998. On the actions that one nerve cell can have on another: distinguishing "drivers" from "modulators". Proc Natl Acad Sci U S A 95: 7121–7126.

Sherwood CC, Raghanti MA, Stimpson CD, Bonar CJ, de Sousa AA, Preuss TM, Hof PR. 2007. Scaling of inhibitory interneurons in areas v1 and v2 of anthropoid primates as revealed by calcium-binding protein immunohistochemistry. Brain Behav Evol 69:176–195.

Shi SR, Key ME, Kalra KL. 1991. Antigen retrieval in formalin-fixed, paraffin-embedded tissues: an enhancement method for immunohistochemical staining based on microwave oven heating of tissue sections. J Histochem Cytochem 39: 741–748.

Shi SR, Cote RJ, Taylor CR. 1997. Antigen retrieval immunohistochemistry: past, present, and future. J Histochem Cytochem 45:327–343.

Solomon SG, Peirce JW, Lennie P. 2004. The impact of suppressive surrounds on chromatic properties of cortical neurons. J Neurosci 24:148–160.

Suurmeijer AJ, Boon ME. 1993. Notes on the application of microwaves for antigen retrieval in paraffin and plastic tissue sections. Eur J Morphol 31:144–150.

Szentagothai J. 1978. The neuron network of the cerebral cortex: a functional interpretation. The Ferrier Lecture 1977. Proc R Soc Lond B 201:219–248.

Trojanowski JQ, Jacobson S. 1976. Areal and laminar distribution of some pulvinar cortical efferents in rhesus monkey. J Comp Neurol 169:371–392.

Takamori S, Rhee JS, Rosenmund C, Jahn R. 2000. Identification of a vesicular glutamate transporter that defines a glutamatergic phenotype in neurons. Nature 407:189–194.

Takamori S, Rhee JS, Rosenmund C, Jahn R. 2001. Identification of differentiation-associated brain-specific phosphate transporter as a second vesicular glutamate transporter (VGLUT2). J Neurosci 21:RC182.

Takamori S, Malherbe P, Broger C, Jahn R. 2002. Molecular cloning and functional characterization of human vesicular glutamate transporter 3. EMBO Rep 3:798–803.

Tigges J, Tigges M. 1979. Ocular dominance columns in the striate cortex of chimpanzee (*Pan troglodytes*). Brain Res 166:386–390.

Unal-Cevik I, Kilinc M, Gursoy-Ozdemir Y, Gurer G, Dalkara T. 2004. Loss of NeuN immunoreactivity after cerebral ischemia does not indicate neuronal cell loss: a cautionary note. Brain Res 1015:169–174.

Varoqui H, Schafer MK, Zhu H, Weihe E, Erickson JD. 2002. Identification of the differentiation-associated Na+/PI transporter as a novel vesicular glutamate transporter expressed in a distinct set of glutamatergic synapses. J Neurosci 22:142–155.

Weber JT, Huerta MF, Kaas JH, Harting JK. 1983. The projections of the lateral geniculate nucleus of the squirrel monkey: studies of the interlaminar zones and the S layers. J Comp Neurol 213:135–145.

Wiesel TN, Hubel DH, Lam DM. 1974. Autoradiographic demonstration of ocular-dominance columns in the monkey striate cortex by means of transneuronal transport. Brain Res 79:273–279.

Wong-Riley M. 1979. Changes in the visual system of monocularly sutured or enucleated cats demonstrable with cytochrome oxidase histochemistry. Brain Res 171:11–28.

Wong-Riley MT, Hevner RF, Cutlan R, Earnest M, Egan R, Frost J, Nguyen T. 1993. Cytochrome oxidase in the human visual cortex: distribution in the developing and the adult brain. Vis Neurosci 10:41–58.

Wong P, Kaas JH. 2008. Architectonic subdivisions of neocortex in the gray squirrel (*Sciurus carolinensis*). Anat Rec (Hoboken) 291:1301–1333.

Wong P, Kaas JH. 2009. Architectonic subdivisions of neocortex in the tree shrew (*Tupaia belangeri*). Anat Rec (Hoboken) 292:994–1027.

Xing D, Ringach DL, Shapley R, Hawken MJ. 2004. Correlation of local and global orientation and spatial frequency tuning in macaque V1. J Physiol 557:923–933.

Yoshioka T, Hendry SH. 1995. Compartmental organization of layer IVA in human primary visual cortex. J Comp Neurol 359:213–220.